Department of Applied Physics

Dynamics of Escape and Translocation of Biopolymers

Timo Ikonen

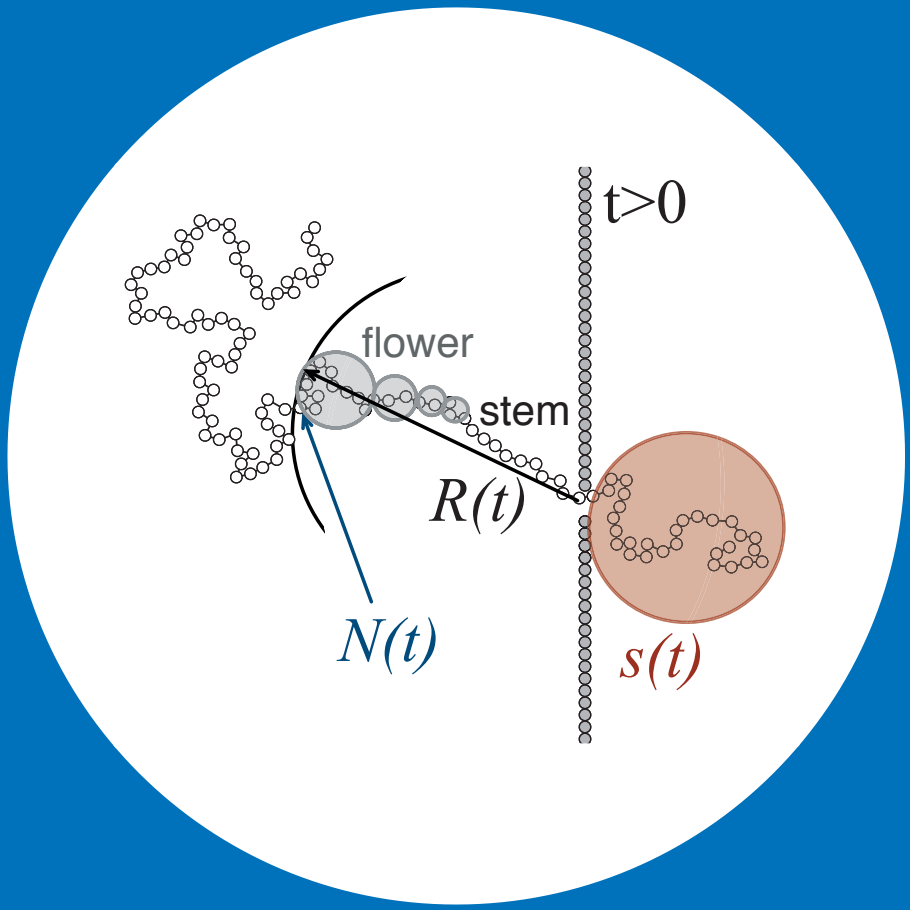

Aalto University

DOCTORAL DISSERTATIONS

Aalto University publication series
DOCTORAL DISSERTATIONS 72/2012

Dynamics of Escape and Translocation of Biopolymers

Timo Ikonen

Doctoral dissertation for the degree of Doctor of Science in Technology to be presented with due permission of the School of Science for public examination and debate in Auditorium K at the Aalto University School of Science (Espoo, Finland) on the 8th of June 2012 at one o'clock.

Aalto University
School of Science
Department of Applied Physics
Multiscale Statistical Physics

Supervisors
Prof. Tapio Ala-Nissilä

Preliminary examiners
Dr. Francesco Montalenti, University of Milano-Bicocca, Italy
Prof. Ralf Metzler, University of Potsdam, Germany

Opponent
Prof. Dieter Heermann, University of Heidelberg, Germany

Aalto University publication series
DOCTORAL DISSERTATIONS 72/2012

ISBN 978-952-60-4646-4 (printed)
ISBN 978-952-60-4647-1 (pdf)
ISSN-L 1799-4934
ISSN 1799-4934 (printed)
ISSN 1799-4942 (pdf)

Unigrafia Oy
Helsinki 2012

Finland

The dissertation can be read at http://lib.tkk.fi/Diss/

Publication orders (printed book):
timo.ikonen@aalto.fi

Aalto University

Abstract

Aalto University, P.O. Box 11000, FI-00076 Aalto www.aalto.fi

Author
Timo Ikonen

Name of the doctoral dissertation
Dynamics of Escape and Translocation of Biopolymers

Publisher School of Science

Unit Department of Applied Physics

Series Aalto University publication series DOCTORAL DISSERTATIONS 72/2012

Field of research Engineering Physics, Theoretical and Computational Physics

Manuscript submitted 17 April 2012 **Manuscript revised** 7 May 2012

Date of the defence 8 June 2012 **Language** English

☐ **Monograph** ☒ **Article dissertation (summary + original articles)**

Abstract

The properties and dynamical behavior of polymers define and enable several processes that occur in biological systems, including the storage and duplication of genetic information in cells. Many such processes are also of considerable technological interest. For example, the driven translocation of a DNA polymer through a nano-sized pore is envisioned as a method of ultra-fast and inexpensive DNA sequencing, which may lead to revolutionary advances in medicine and biotechnology.

In this dissertation, dynamics of polymers is studied in two related contexts. The first part of the thesis discusses the escape of polymers from a metastable state, which is studied with an accelerated Langevin dynamics method, the so-called Path Integral Hyperdynamics. In the same context, the method itself and its performance is studied. The results suggest that efficient separation of polymers by length or bending rigidity may be possible using external potentials.

In the second part of the thesis, the driven translocation of polymers is studied. A theoretical model of the process is proposed, and its predictions are compared with molecular dynamics (MD) simulations. It is shown conclusively that the dynamics of driven translocation can be described by a two-stage process, where the polymer first straightens due to the driving force, and is thereafter effectively shortened as it threads through the pore. Furthermore, the effect of the pore and other finite size effects to the dynamical scaling of the process is discussed. Finally, driven translocation under time-dependent force is investigated with MD simulations. It is shown that for sufficiently strong attractive interactions between the pore and the polymer, the translocation becomes a thermally activated process similar to the polymer escape, and can exhibit the so-called resonant activation phenomenon. In the resonance, the translocation time attains a global minimum, which may be beneficial for, e.g., sorting and identification of polymers.

Keywords Molecular dynamics, Soft matter, Rare events, Polymer translocation, Hyperdynamics, Resonant activation

ISBN (printed) 978-952-60-4646-4 **ISBN (pdf)** 978-952-60-4647-1

ISSN-L 1799-4934 **ISSN (printed)** 1799-4934 **ISSN (pdf)** 1799-4942

Location of publisher Espoo **Location of printing** Helsinki **Year** 2012

Pages 145 **The dissertation can be read at** http://lib.tkk.fi/Diss/

Aalto-yliopisto

Tiivistelmä

Aalto-yliopisto, PL 11000, 00076 Aalto www.aalto.fi

Tekijä
Timo Ikonen

Väitöskirjan nimi
Biopolymeerien pako- ja translokaatiodynamiikka

Julkaisija Perustieteiden korkeakoulu

Yksikkö Teknillisen fysiikan laitos

Sarja Aalto University publication series DOCTORAL DISSERTATIONS 72/2012

Tutkimusala Teknillinen fysiikka, teoreettinen ja laskennallinen fysiikka

Käsikirjoituksen pvm 17.04.2012 **Korjatun käsikirjoituksen pvm** 07.05.2012

Väitöspäivä 08.06.2012 **Kieli** Englanti

☐ **Monografia** ☒ **Yhdistelmäväitöskirja (yhteenveto-osa + erillisartikkelit)**

Tiivistelmä

Biologisissa systeemeissä polymeerien ominaisuudet ja dynamiikka ohjaavat ja mahdollistavat useita prosesseja, kuten soluissa tapahtuvan geneettisen tiedon tallentamisen ja monistamisen. Monilla tällaisilla prosesseilla on myös mielenkiintoisia teknologiasovelluksia. Esimerkiksi DNA-polymeerin ajetun translokaation nanokokoisen huokosen läpi uskotaan mahdollistavan ultranopean ja edullisen DNA:n sekvensoinnin, mikä saattaa johtaa mullistaviin edistysaskeliin lääketieteessä ja bioteknologiassa.

Tässä väitöstyössä polymeerien dynamiikkaa tutkitaan kahdessa toisiinsa liittyvässä tapauksessa. Väitöskirjan ensimmäisessä osassa tarkastellaan polymeerien pakenemista metastabiilista tilasta käyttämällä kiihdytettyä Langevin-dynamiikkaa, ns. polkuintegraalihyperdynamiikkamenetelmää. Tässä yhteydessä tutkitaan myös itse menetelmää ja sen ominaisuuksia. Tulosten valossa polymeerien erotteleminen pituuden ja jäykkyyden perusteella voi olla mahdollista esim. ulkoisia potentiaaleja käyttäen.

Väitöskirjan toisessa osassa tutkitaan ulkoisella voimalla ajettua polymeeritranslokaatiota. Prosessin kuvaamiseksi esitetään teoreettinen malli, jonka ennusteita verrataan molekyylidynamiikkasimulaatioihin. Tulokset osoittavat, että ajetun translokaation dynamiikkaa voidaan kuvata kaksivaiheisena prosessina, jossa ajava voima ensin suoristaa polymeerin, joka sitten toisessa vaiheessa efektiivisesti lyhenee pujottautuessaan huokosen läpi. Lisäksi työssä tarkastellaan huokosen ja polymeerin välistä vuorovaikutusta sekä muita äärellisen koon vaikutuksia prosessin dynaamiseen skaalaukseen. Lopuksi ajasta riippuvalla voimalla ajettua translokaatiota tutkitaan molekyylidynamiikkasimulaatioilla. Työssä osoitetaan, että mikäli huokosen ja polymeerin välillä on riittävän voimakas puoleensavetävä vuorovaikutus, translokaatiosta tulee polymeerin pakenemisen kaltainen termisesti aktivoitu prosessi, jolloin ns. resonantti aktivoituminen tulee mahdolliseksi. Resonanssissa translokaatioaika minimoituu, mitä voi olla mahdollista hyödyntää esim. polymeerien lajittelussa ja tunnistamisessa.

Avainsanat Molekyylidynamiikka, Pehmeä aine, Harvinaiset tapahtumat, Polymeeritranslokaatio, Hyperdynamiikka, Resonantti aktivoituminen

ISBN (painettu) 978-952-60-4646-4 **ISBN (pdf)** 978-952-60-4647-1

ISSN-L 1799-4934 **ISSN (painettu)** 1799-4934 **ISSN (pdf)** 1799-4942

Julkaisupaikka Espoo **Painopaikka** Helsinki **Vuosi** 2012

Sivumäärä 145 **Luettavissa verkossa osoitteessa** http://lib.tkk.fi/Diss/

Preface

The work presented in this Thesis has been carried out in the Multiscale Statistical Physics group at Aalto University School of Science. The work has been supported by the Academy of Finland's Center of Excellence in Computational Nanoscience (COMP), the Finnish Cultural Foundation, the Finnish Foundation for Technology Promotion, the Finnish Doctoral Programme in Computational Sciences (FICS), and CSC IT Center for Science.

I sincerely wish to thank my supervisor and advisor, prof. Tapio Ala-Nissilä, for the opportunity to work and carry out my doctoral studies in his group. I am especially grateful to Tapio for always being very optimistic and pushing me forward at the right moment, when I might have given up otherwise. I also want to thank Tapio for being open to my ideas and encouraging individual thinking, which certainly has helped me to stand on my own as a scientist. In addition to his moral and scientific support, Tapio also provided us students with an extensive network of collaborators and visiting researchers, which has proven an invaluable resource, and has also taught me the value of good collaborations in a very hands-on way.

I also wish to thank all the people I've had the pleasure of collaborating with during the last four years. During the first two years, I had several good discussions with prof. See-Chen Ying, who helped me to grasp the essentials of a field that at the time was largely unknown to me. I also want to give big thanks to prof. Wokyung Sung for his mentoring and hospitality during my visit to Pohang in the beginning of 2011, which, looking back, was a turning-point in my thesis research. A big thanks also goes to Jaeoh Shin for extremely fruitful and effortless collaboration on several topics. I also wish to thank prof. Aniket Bhattacharya for his generous hospitality during my visits in the spring of 2011 and 2012, and

for his insight on both the science of polymer translocation and the art of scientific communication. Finally, I want to extend my thanks to prof. Hannes Jónsson for inspiring discussions regarding escape problems and for giving feedback on the manuscript of this Thesis.

Although too numerous to mention by name, I wish to thank all of my friends, both at the office and outside of work. For the guys at the office, thanks for the entertaining discussions, both related to work and (most often) not. Thanks for creating a relaxed atmosphere where it has been easy and pleasant to work in. Also thanks to my friends outside the office, both physicists and non-physicists, for the much-needed distractions, and my apologies for the occasional ramblings caused by thesis anxiety. I promise to cock a sympathetic ear when you are in a similar situation.

Thinking back, I do not think I would be writing this preface if it weren't for the support of my parents. Their support and belief in my choices in all areas of life seems unwavering, and they have always been there in times of need. For that and everything, they have my gratitude.

Last, but certainly not least, the biggest thanks of all goes to my beloved wife Reetta. Thank you for understanding my passion for physics, enduring the times when this Thesis required a bit too much of my attention, and for loving me nonetheless. Know that without you, this accomplishment and life itself would seem hollow and without meaning. Thank you.

Espoo, May 7, 2012,

Timo Ikonen

Contents

List of Publications

This thesis consists of an overview and of the following publications which are referred to in the text by their Roman numerals.

I T. Ikonen, M.D. Khandkar, L.Y.Chen, S.C. Ying and T. Ala-Nissila. Diffusion in periodic potentials with path integral hyperdynamics. *Physical Review E*, 84, 026703-1–026073-7, August 2011.

II Jaeoh Shin, Timo Ikonen, Mahendra D. Khandkar, Tapio Ala-Nissila and Wokyung Sung. Polymer escape from a metastable Kramers potential: Path integral hyperdynamics study. *The Journal of Chemical Physics*, 133, 184902-1–184902-7, November 2010.

III T. Ikonen, A. Bhattacharya, T. Ala-Nissila and W. Sung. Unifying model of driven polymer translocation. Accepted for publication in *Physical Review E*, April 2012.

IV T. Ikonen, A. Bhattacharya, T. Ala-Nissila and W. Sung. Influence of non-universal effects on dynamical scaling in driven polymer translocation. *The Journal of Chemical Physics*, submitted April 2012.

V Timo Ikonen, Jaeoh Shin, Tapio Ala-Nissila and Wokyung Sung. Polymer translocation under time-dependent driving forces: resonant activation induced by attractive polymer-pore interactions. *The Journal of Chemical Physics*, submitted February 2012.

Author's Contribution

Publication I: "Diffusion in periodic potentials with path integral hyperdynamics"

The author did the numerical simulations and analytical calculations. The author co-wrote the manuscript.

Publication II: "Polymer escape from a metastable Kramers potential: Path integral hyperdynamics study"

The author did part of the numerical simulations, co-wrote the first version of the manuscript and participated in interpreting the results.

Publication III: "Unifying model of driven polymer translocation"

The author derived the final model and did the analytical and numerical calculations. The author interpreted the results and wrote the first version of the manuscript.

Publication IV: "Influence of non-universal effects on dynamical scaling in driven polymer translocation"

The author did the analytical and numerical calculations and simulations, and wrote the first version of the manuscript.

Publication V: "Polymer translocation under time-dependent driving forces: resonant activation induced by attractive polymer-pore interactions"

The author did half of the numerical simulations and participated in interpreting the results. The author co-wrote the first version of the manuscript.

1. Introduction and background

1.1 Introduction

All life on Earth shares the same code for storing genetic information. This hereditary code that holds the instructions to the organism's development and functions, is contained in a molecule called DNA (or RNA for certain viruses). The DNA is a double-stranded polymer, each strand composed of four different kinds of repeating units, nucleotides. When arranged in a sequence, the nucleotides form a genetic code that can be read by biological organelles to produce various functions within the living cell, or by technological means to obtain information about the organism. The technological process of extracting the information contained in the DNA is called DNA sequencing. The term covers a variety of different methods developed since the 1970's to understand the genetic makeup of living beings, and even after 40 years, the field is growing at an increasing rate. The reason is that unlocking the complete genetic code allows remarkable advances in biotechnology, food production, medicine, forensics, and beyond.

Although the first sequencing methods were developed already in the beginning of the 1970's, the initial progress was slow, especially in obtaining complete DNA sequences of organisms. While the complete DNA genome of the bacteriophage ϕX174 was sequenced already in 1977 [1], the first complete genome of a free-living bacterium was not obtained until almost 20 years later [2]. The human genome was published six years later in 2001, after ten years of work and a price tag of almost 3 billion dollars [3, 4, 5]. The main reason for the slow initial progress and high costs were the limitations of the early sequencing methods. The methods consist of several steps, where the DNA is first split into smaller frag-

ments, each of which is replicated to produce several copies that are then analyzed to give the sequence of the given fragment. The same process is repeated for all the fragments, and in post processing the fragment data is combined by looking for overlaps in the subsequent fragments. Typically, the DNA has to be assembled from at least several million of such fragments, which makes the task slow, expensive and computationally challenging. Since 2007, the advent of the so-called second generation sequencing methods have made the process considerably faster and cheaper, with the sequencing of the human genome taking less than a week and costing roughly ten thousand dollars in 2010 [5, 6]. Although the second generation methods allow for massively parallelized sequencing, the maximum size of the fragment is still very limited (even more strictly than in the first generation devices), which means that the DNA sequencing time and cost will eventually be limited by advances in computational algorithms and hardware [5].

At present, in 2012, the third generation of DNA sequencers is beginning to make its entrance to the market. Although several alternative concepts are under development, one of the most promising is the so-called nanopore sequencing. In this method, a single DNA polymer is pulled through a nano-sized pore, which produces a measurable signal in, e.g., the electric current that flows through the pore (see Figure 1.1). The different nucleotides, because of their dissimilar physical and chemical properties, give a characteristic disruption in the current, in principle allowing identification of different sequences [7, 8]. If sufficient accuracy is achieved with such a method, it will have several advantages over the presently available technologies [5, 9]. Because the sequencing can be done using a single molecule, instead of using numerous copies, many of the preparatory steps necessary in conventional methods can be avoided. This saves a significant amount of both time and money. In addition, considerably longer fragments can be used compared to the present methods, which reduces the post processing requirements considerably, especially if the genome is sequenced *de novo*, without the necessity to refer to archived sequencing data for the same organism. The process is also very scalable, allowing massively parallel sequencing with nanopore arrays.

The overall potential with nanopore sequencing is enormous. Recently (in February 2012), Oxford Nanopore Technologies, an Oxford based company, announced that they will bring a nanopore-based sequencer to the market in 2012 [10]. According to the company, both the speed and the

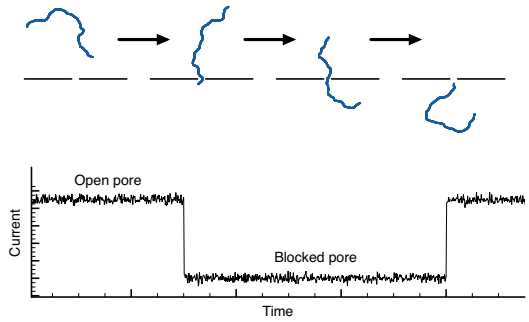

Figure 1.1. Schematic presentation of DNA sequencing by translocation of DNA through a nanopore. When the pore is open, an electric current passes through the pore from one side of the membrane to the other. When a polymer enters the pore, part of the current is blocked, which gives a detectable signal. The strength of the signal depends on the type of the DNA's nucleotide, in principle allowing sequencing of DNA by monitoring the current flowing through the pore.

cost of the nanopore sequencer will be competitive with the presently available technologies. By using several of their platforms in parallel, they expect that it may be possible to sequence the human genome in as little as 15 minutes, although this would result in a higher monetary cost. In general, the target cost of 100 dollars for sequencing the human genome is nowadays considered to be a reasonable goal [5]. This kind of price combined with the sequencing time of hours (or even minutes,) instead of days, could make DNA sequencing as commonplace as regular blood tests are today. This kind of availability to the general practitioner could potentially revolutionize modern medicine, allowing personalized medical treatments tailored for the individual patient. In the future, accurate and preventive diagnosis of, e.g., hereditary diseases and cancers could be possible at modest cost.

However, the nanopore technology of DNA sequencing is still in its early stages and far from realizing its full potential. At the moment, several alternative technical solutions are explored. For example, some approaches use an enzyme at the entrance of the nanopore to cleave the nucleotides off the DNA strand. The nucleotides are then measured individually inside the pore. An alternative method is to sequence the DNA as an intact strand as it translocates through the nanopore [9]. The former method is less sensitive to measurement noise due to the lack of interference from the neighboring nucleotides, while the latter has the advantage of higher potential throughput.

Aside from the many technical details of nanopore sequencing, even

some fundamental physical questions remain open. Until very recently, even the correct physical description of polymer translocation under an external driving force was unknown. This remained not only a serious theoretical issue, but also a practical problem for the experimentalists working on polymer translocation, since a thorough understanding and preparation of experiments always requires solid theoretical knowledge on the subject. As a part of this Thesis, a unifying theory of the physics of driven polymer translocation is presented. The theory allows an extremely lucid description of the underlying physics and, hopefully, will inspire further discoveries in polymer translocation, both experimental and theoretical.

The rest of this Thesis is organized as follows. In Section 1.2 we discuss the general class of physics problems known as thermally activated processes, which include such processes as chemical reactions, surface diffusion, polymer escape and, in some cases, polymer translocation. The polymer translocation problem is introduced in Section 1.4, although more detailed discussion about the theory of driven polymer translocation is given later in the Thesis. In Chapter 2 we discuss the problem of thermally activated escape of polymer from a metastable state, and a computational method called Path Integral Hyperdynamics that can be used to significantly accelerate simulations of such problems. In this context, we also give an overview of the results of Publications I & II. Chapter 3 presents the central results of Publications III, IV & V. Section 3.1 gives an overview of the current state-of-the-art theory of driven polymer translocation, which is presented in Publications III & IV. Finally, in Section 3.2, we discuss polymer translocation under time-dependent force in the regime, where the theory discussed in the preceding Section is not valid, and summarize the results of Publication V.

1.2 Thermally activated processes

1.2.1 The Langevin equation

Many problems in chemistry, physics, biology and engineering involve transitions of the system from an initial state to some other state. Examples of such processes include protein folding, surface diffusion (hopping of an adatom from one lattice site to the next), chemical reactions and

electron transport in semiconductors [11, 12]. Within classical physics, such processes are described by Brownian motion in an external potential, where the system escapes from the initial metastable state due to thermal fluctuations. Mathematically, such processes can be described by, e.g., the Fokker-Planck equation [13], or the Langevin equation,

$$m\ddot{x} = -m\eta\dot{x} - \nabla U(x) + \zeta(t). \tag{1.1}$$

The Langevin equation in Eq. (1.1) is an equation of motion for one particle with mass m moving in an external potential given by $U(x)$, subject to coarse-grained interactions with the thermal environment. The interactions are reduced to the frictional force $-m\eta\dot{x}$ and the random force $\zeta(t)$. The random is typically taken to be Gaussian white noise with mean $\langle\zeta(t)\rangle = 0$ and correlations $\langle\zeta(t)\zeta(t') = 2k_BTm\eta\delta(t-t')$. Here, the average $\langle\cdot\rangle$ is taken over the different realizations of the random force, and k_B is the Boltzmann constant, T is the absolute temperature, η is the friction coefficient and $\delta(t)$ is the Dirac delta function. Together the friction and the random force satisfy the fluctuation-dissipation theorem, acting as a thermostat for the system. In many cases, the Langevin equation is further approximated by considering the overdamped limit, where the inertial term $m\ddot{x}$ is neglected from Eq. (1.1). The Langevin equation will be used extensively in this Thesis to describe coarse-grained dynamics of particles and polymers.

1.2.2 Kramers' escape rate

In the context of thermally activated processes, the central issue is to calculate the escape rate k from the metastable state. Since the initial state is metastable, its population (or the probability that the system is in the initial state) is approximately constant only on time-scales that are short compared to the escape rate. Therefore the escape rate, which depends on the system's probability distribution, is in general also a function of time. For example, to calculate the reaction rate $\mathbf{k}_{A\to B}$ from the reactant state A to the product state B, one has to calculate the time-dependent rate $\mathbf{k}(t)$ defined as [15, 16]

$$\mathbf{k}(t) = \frac{d}{dt}\frac{\langle h_A(0)h_B(t)\rangle}{\langle h_A(0)\rangle} \approx \mathbf{k}_{A\to B}e^{-t/t_{\text{rxn}}}, \tag{1.2}$$

where h_A and h_B are the characteristic functions defined as

$$h_{A,B}(t) = \begin{cases} 1, \text{ if } x(t) \in A, B \\ 0, \text{ if } x(t) \notin A, B \end{cases}, \tag{1.3}$$

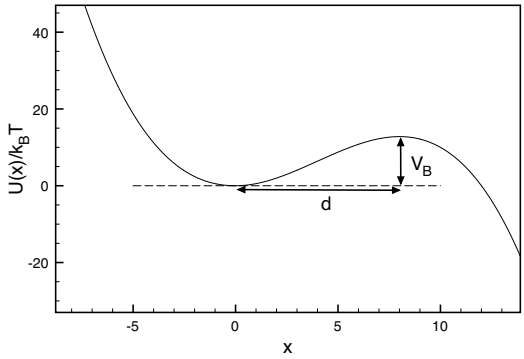

Figure 1.2. Schematic illustration of the metastable potential typical of the Kramers problem. The metastable minimum of the potential is located at $x = 0$ and the local maximum (the barrier) at $x = d$. The difference in potential energy between the local minimum and maximum (the barrier height) is V_B.

and $t_{\rm rxn} = (\mathrm{k}_{A\to B} + \mathrm{k}_{B\to A})^{-1}$ is the relaxation time related to the forward ($\mathrm{k}_{A\to B}$) and backward ($\mathrm{k}_{B\to A}$) reaction rates. In this Thesis, unless otherwise indicated, when discussing the escape rate from, say, state A to state B, we refer to the time-independent rate $\mathrm{k}_{A\to B}$, which is valid for timescales shorter than t_{rxn}.

The separation of time scales between the equilibration time of the system in the metastable state and the relaxation time t_{rxn} was first appreciated in the context of mathematically formulated reaction rate theory by Kramers in 1940 [14]. Kramers modeled the general chemical reaction using a simplified model of one reaction coordinate, x, for which he solved the escape rate in an external metastable potential. In the high barrier limit, $V_B/k_BT \gg 1$, one can employ the saddle-point approximation to get the famous Kramers rate for thermally activated escape across the barrier [13, 14],

$$\mathrm{k} = \frac{\omega_0\omega_B}{2\pi\eta} e^{-\beta V_B}. \tag{1.4}$$

In Eq. (1.4), $\beta = 1/k_BT$ is the inverse temperature, V_B is the height of the barrier (see Figure 1.2) and ω_0 and ω_B denote the square root of $m^{-1}\frac{d^2U(x)}{dx^2}$ evaluated at the bottom of the metastable well ($x = 0$) and at the barrier top ($x = d$), respectively. The formula includes the exponential dependence of the rate on the height of the activation barrier and inverse temperature, which was postulated on experimental basis by Arrhenius already in 1889. In addition, Kramers was able to derive the prefactor, which includes the vibrational frequency of the stable mode at the bottom of the well, ω_0, and the corresponding frequency of the unstable mode at the barrier top, ω_B. The formula of Eq. (1.4) is valid in the high barrier

($V_B \gg k_B T$) and high friction ($\eta \gg \omega_B$) regime. The former guarantees that the intrawell relaxation time is much shorter than the escape time, hence the probability distribution of the initial state is given by the Boltzmann distribution. The latter criterion ensures that the system's time evolution is stochastic rather than ballistic, and is required to write down the equation of motion of the probability distribution in the Fokker-Planck form [13, 17]. The rate can also be solved in the low-friction limit, by writing down the diffusion equation for the action [14, 17]. In a more complex system, Kramers' theory also neglects the recrossings due to a multidimensional energy landscape, including only the recrossing due to thermal fluctuations.

1.2.3 Hyperdynamics

Although the Kramers' rate, Eq. (1.4), gives a very good approximation of the reaction rate for many systems, in practice it is seldom possible to apply it directly. In some cases of interest, all of its assumptions may not be valid. Furthermore, in high-dimensional, many-particle systems, obtaining the free energy along the reaction coordinate can be difficult, and often even defining a suitable reaction coordinate is challenging, due to the complex free energy landscape and several possible reaction pathways. Therefore, in many cases the reactions need to be calculated using, e.g., numerical Monte Carlo or molecular dynamics (MD) simulations to obtain the rates. The rates can be obtained by, e.g., calculating the correlation function $\langle h_A(0) h_B(t) \rangle$ of Eq. (1.2), or by calculating the flux through the dividing surface that separates the product state from the reactant state. The latter method is the so-called transition state theory (TST) approximation, which gives an upper bound for the rate, although in many cases it is very close to the true rate [15, 17].

A common limitation in numerical studies of physics or chemistry is the availability of computer resources. This is especially true of escape processes, where the reaction rates can be extremely low at the relevant temperatures. The occasional crossing event occurs extremely rarely, requiring very long simulation times to observe even a few of these events. Obtaining reliable statistical accuracy is in such cases impossible with conventional simulation techniques. To speed up the simulation of these rare events, Voter introduced the so-called hyper-MD, or hyperdynamics, method in 1997 [18]. The idea is similar to the various importance sampling methods in Monte Carlo simulations, where the states of the system

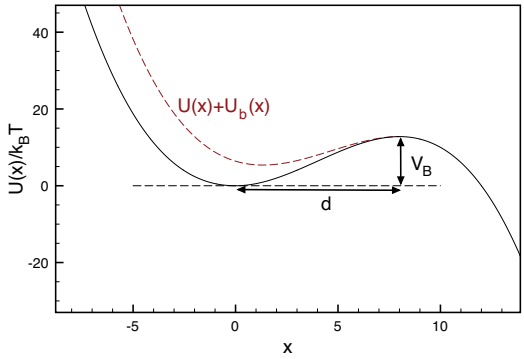

Figure 1.3. Illustration of the principle of the hyperdynamics method. The system's crossing dynamics is accelerated by addition of a bias potential $U_b(X)$, which lowers potential barrier and boosts the number of crossings per unit time. The dynamics is afterwards corrected back to the original system.

are sampled under a modified external potential for better ergodicity, and the statistical weight of the sampling is corrected afterwards [19]. In the hyperdynamics method, the dynamics of the system is artificially accelerated by modifying the external potential with a so-called *bias potential* so that the crossings become more frequent (see Figure 1.3). In Voter's original method, the accelerated dynamics is afterwards mapped back to the original system by making the simulation time a statistical quantity. Although the simulation time in the biased system advances with constant time steps, the corresponding time in the unbiased (original) system is calculated as

$$t_{\mathrm{HD}} = \sum_{i}^{n_{\mathrm{tot}}} \delta t_{\mathrm{HD},i} \; ; \quad \delta t_{\mathrm{HD},i} = \delta t_{\mathrm{MD}} e^{\beta U_b[x(t_i)]}, \tag{1.5}$$

where δt_{MD} is the MD time step, n_{tot} is the total number of MD steps, and t_i indicates the time at the ith MD step.

The original hyperdynamics method of Voter is based on the TST approximation of activated processes, and therefore has the same limitations. Essentially, this means that the obtained rate is always an upper bound, the quality of which is somewhat sensitive to the choice of the dividing surface. In addition, the bias potential $U_b(x)$ has to go to zero at the transition state. Since the original hyperdynamics method, other alternative schemes have been developed for different purposes (see, e.g., Refs [20, 21] and references therein). In this Thesis, a novel formulation of the hyperdynamics type methods is studied and further developed. The method is based on the path integral formulation of Langevin dynamics and was first published by Chen and Horing [21] in 2007. This Path Inte-

gral Hyperdynamics (PIHD) method is described in detail in Section 2.2 and in Publications I & II. In this context, we merely mention that it has several advantages over the previous hyperdynamics methods. The method gives an exact correction to accelerated dynamics, and is not limited by the approximations of the transition state theory. It is also very flexible, allowing virtually any kind of potential, even time dependent, to be used as a bias.

1.2.4 Resonant activation

Because of the exponential dependence of the crossing rate on the barrier height (cf. Eq. 1.4), the system can exhibit interesting behavior if the barrier height is modulated in time. In 1992, Doering and Gadoua [22] studied a somewhat similar system of two metastable states separated by a triangular potential barrier, whose height changes dichotomically with time. They found that the barrier crossing is most likely to occur when the barrier is the lower state and that the barrier crossing rate can be greatly enhanced by the non-equilibrium dichotomic noise at the resonant flipping rate [22]. This phenomenon is called resonant activation. Since its discovery, the resonant activation phenomenon has been studied and analyzed by several authors (see, e.g., Refs [23, 24] for discussions of its general properties).

The resonant activation phenomenon and the existence of a maximum crossing rate can be understood as follows. Suppose the system is initially in the metastable state at temperature k_BT. The system's activation barrier changes dichotomically in time between the upper state of $V_B + A$ and the lower state $V_B - A$ with mean flipping rate ω (see Figure 1.4). If the temperature is sufficiently low, $k_BT \ll V_B + A$, the system is very unlikely to cross the activation barrier if the barrier is in its upper state. For extremely low flipping rates of the dichotomic force, the system may have to wait for a very long time until either the barrier flips to its lower state, or sufficient thermal fluctuations activate the system across the barrier. In the low flipping rate limit, the mean residence time τ (the time that the system has to wait before the transition occurs) is given by the weighted average $\tau = p_+\tau_+ + p_-\tau_-$, where p_+ (p_-) is the probability that the barrier is initially in the upper (lower) state and τ_+ (τ_-) is the residence time with the barrier in the upper (lower) state. Since $\tau_\pm \sim e^{-\beta(V_B \pm A)}$, the mean residence time τ is dominated by τ_+, unless the probability p_+ decreases exponentially with increasing A. Therefore, in the low flipping

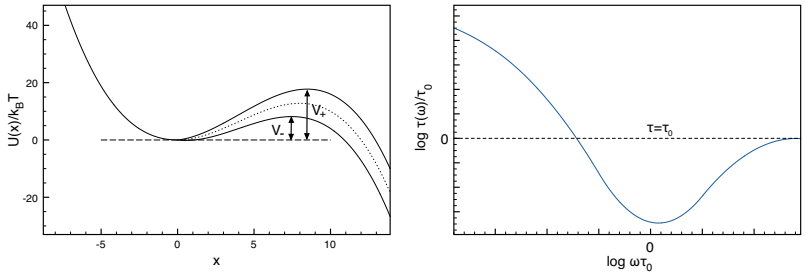

Figure 1.4. Left panel: The potential of Figure 1.2 with the height of the barrier modulated in time between $V_+ = V_B + A$ and $V_- = V_B - A$ gives rise to the resonant activation phenomenon (see text). Right panel: For a matching barrier crossing rate and barrier flipping rate ω, the residence time τ in the metastable well is minimized (schematic illustration). The mean residence time in the absence of the time-dependent barrier modulation is τ_0.

rate limit, the mean residence time is typically longer than the residence time in the absence of the dichotomic fluctuations, $\tau > \tau_0$ (see Figure 1.4).

In the opposite limit of very fast flipping ($\omega \gg 1/\tau_0$), the dynamics of the system is much slower than the barrier flipping rate. Hence, the crossing event seldom occurs within a time period of constant barrier height. Instead, the height of the barrier changes several times during the crossing event. Because of this, the fast fluctuations are averaged out and the residence time is approximately equal to the residence time in absence of the dichotomic fluctuations, $\tau \approx \tau_0$. The equality is not exact, because the effect is non-linear and in principle the dichotomic force acts as an additional source of fluctuations in the system, increasing the system's temperature beyond that of the heat bath. However, in this Thesis we consider cases where this effect is small, and the approximate relation holds well.

In the intermediate regime between the high and low ω regimes, the situation is considerably more interesting. In this regime, the time scale of the barrier crossing dynamics is comparable to the dichotomic flipping rate ($\omega \approx 1/\tau_0$). Thus, the effect of the dichotomic force is not averaged out as in the fast flipping limit. In addition, in this regime, the flipping rate is large compared to the crossing rate with the barrier in the upper state. Therefore, even when the barrier is initially in the unfavorable state at $V_B + A$, the system rarely has to wait the time τ_+ for the thermal fluctuations to initiate the barrier crossing. Instead, the barrier flips to the lower state of $V_B - A$, and the system crosses the lower activation barrier. Therefore, in the intermediate rate regime, the crossing typically occurs when the barrier is in the lower position. This is in contrast to the low and

high flipping regimes, where the moment of crossing is only very weakly correlated with the barrier flipping dynamics. Because the crossing typically occurs when the barrier is in the lower position, the mean residence time is dominated by the time τ_-, and the overall residence time is shorter than without the dichotomic fluctuations, $\tau < \tau_0$. The flipping rate corresponding to the minimum residence time is called the resonant flipping rate. However, because the crossing may occur with finite probability also when the barrier is in the upper state, the resonance is typically quite broad, possibly even several orders of magnitude in the ω axis.

1.3 Polymer escape

Thermally activated processes are also important in polymer physics, and they appear in many contexts, such as electrophoresis, transport through nanochannels, various biological cell functions and in polymer translocation. Also for the polymer, the Kramers type escape process from a single metastable well can be viewed as the simplest prototype of a thermally activated process. In the case of the polymer, the flexibility and extensibility of the chain makes the situation considerably more complicated. Due to the freedom of the chain to assume different configurations, the free energy of the system may contain a significant contribution from the polymer's configurational entropy, in addition to the external potential such as shown in Figure 1.2.

The polymer escape problem has been analyzed analytically by several authors, using the so-called ideal chain model, where the polymer consists of dimensionless monomers interconnected with massless springs that can freely intersect each other [25, 26, 28, 29]. Using such models, it is been possible to formulate the Kramers escape problem for the ideal polymer and derive analytical results for, e.g., the crossing rate of the polymer. One quantity of interest is the escape rate as a function of chain length. Due to the entropic part of the free energy, the escape rate can be a non-monotonic function of chain length, which is important for, e.g., separation of polymers by their chain length (or molecular mass).

In many cases, however, important details may be overlooked by simplified models such as the ideal chain model. For example, in a real polymer the monomers cannot overlap and the bonds cannot intersect: the volume occupied by one monomer is excluded from the others. Polymer models with such *excluded volume* interactions are called *self-avoiding*

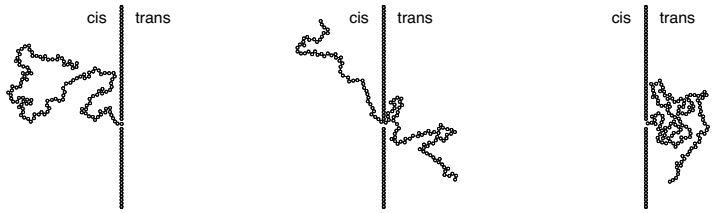

Figure 1.5. An illustration of the polymer translocation process. The polymer is initially on the *cis* side. The translocation event starts when a part of the polymer enters the pore (left panel). The polymer then threads through the pore (middle panel) until it is completely on the *trans* side, at which point the process ends (right panel).

polymers [30]. While in many respects the self-avoiding polymer is similar to the ideal polymer, they can behave very differently in, e.g., confined geometries. For the ideal polymer, it is possible to compress the polymer into an almost point-like volume, while for the self-avoiding polymer, the energy due to the excluded volume interactions quickly diverges under compression. Similarly for the Kramers escape problem, where the polymer is confined in the metastable well formed by the external potential, one expects to find very different behavior for the ideal and self-avoiding chains when the size of the well is comparable to the size of the polymer. Unfortunately, the dynamics of self-avoiding polymers is extremely difficult to study analytically due to the many-body excluded volume interactions. Thus, in this Thesis, the polymer escape problem is studied by numerical simulations, using the Path Integral Hyperdynamics method, which is derived in Chapter 2 and whose properties are discussed in the same Chapter and in Publication I. The results and their implications are presented in Publication II and in Chapter 2.

1.4 Polymer translocation

The polymer translocation is a process, where the polymer, immersed in a solvent, threads through a nano-size pore from one side of a wall (e.g., a cellular membrane or an artificial structure) to the other. In its initial state, the polymer is in its entirety on the *cis* side of the wall, while in the final state, it is completely on the *trans* side (see Figure 1.5). While the problem shares many similarities with the escape problem, it has a few important differences.

While in polymer escape, the external potential may be even the dominant contribution to the free energy barrier, in the typical polymer translo-

cation problem the barrier is almost entirely of entropic origin[1]. The entropic barrier can be estimated by enumerating the possible configurations the chain can adopt in free space, or when it is partly threaded through the pore. For the ideal chain, the calculation results in the free energy

$$\mathcal{F}(s) = \frac{1}{2}k_B T \ln\left[\frac{s}{a}\left(N - \frac{s}{a}\right)\right] + \frac{s}{a}\Delta\mu, \tag{1.6}$$

which is written as a function of the *translocation coordinate*, s, defined as the length of the chain on the *trans* side. The coordinate s acts as the reaction coordinate for the system. The remaining quantities in Eq. (1.6) are a, the segment length of the polymer, and $\Delta\mu$, which is the chemical potential difference between the *cis* and *trans* sides (and is an energetic contribution to the free energy). The most obvious difference between the free energy of Eq. (1.6) and the Kramers potential (cf. Figure 1.2) is that in the case of translocation, the free energy has no finite minima, as shown in Figure 1.6. Consequently, the system also has no metastable state. In practice, for the experimentally or theoretically relevant polymer lengths N the translocation can only occur if there is a chemical potential difference of $\Delta\mu < 0$ that tilts the free energy towards the *trans* side, as shown in Figure 1.6. Such a chemical potential difference may be caused, e.g., by an electrical field at the pore, produced by placing electrodes in the *cis* and *trans* chambers. This is also the method that is typically used in experiments to drive polymer translocation [9, 31].

Because in the practical experiments the polymer has to be driven through the pore by an external force, this *driven translocation* is the most interesting from the point of view of applications, such as DNA sequencing. The problem is also extremely interesting theoretically. Because the polymer is driven through the pore by a force that is acting locally, the influence of the force on the polymer's configuration is strong. Therefore, driven translocation is fundamentally a problem of non-equilibrium statistical physics, as opposed to the escape problem, which is largely an equilibrium process (remember that the assumption of the Kramers' solution is the separation of time scales and the canonical equilibrium distribution within the metastable state). The non-equilibrium theory of driven polymer translocation is described in Section 3.1 of this Thesis. The Section is an overview of Publications III & IV, where the theory is introduced

[1]The exception to this rule is the case where there are strong attractive interactions between the pore and the polymer, which is discussed in Section 3.2 and in Publication V.

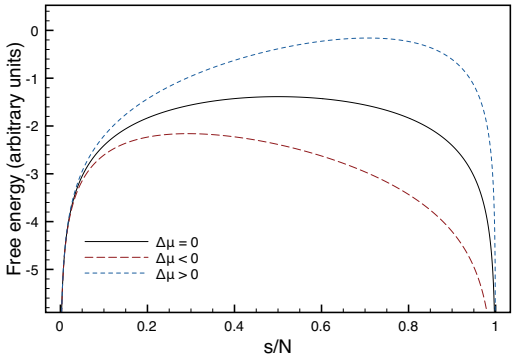

Figure 1.6. The free energy landscape of polymer translocation, displayed as a function of the translocation coordinate s. For the unbiased translocation, the barrier is completely entropic and symmetric. The maximum corresponds to the configurations in which the polymer is half-way through the pore. For nonzero chemical potential difference $\Delta\mu$, the barrier is tilted either towards the *cis* ($\Delta\mu > 0$) or the *trans* side ($\Delta\mu < 0$).

and compared to molecular dynamics simulations.

In some cases, the polymer translocation process can be described as a thermally activated process such as discussed in Section 1.2. This is the case for instance when there are sufficiently strong attractive interactions between the pore and polymer, such that a metastable state is formed. When this occurs, one encounters the phenomena typical of activated processes, such as resonant activation. Studying the resonant activation phenomenon of polymer translocation is the subject of Section 3.2 and Publication V, where it is shown that while the phenomenon shares many similarities with its one-dimensional analogue, there are also important differences, characteristic of polymer translocation.

2. Polymer escape

2.1 Langevin dynamics

As mentioned in Chapter 1, considering polymer models beyond the ideal chain approximation is necessary in many situations. However, due to complicated interactions, treating analytically the dynamics for, e.g., the self-avoiding chain, is typically not possible. Because of this, numerical methods such as molecular dynamics (MD) simulations are needed. In MD simulations, the system's equations of motion are discretized in time and solved by an appropriate numerical integration algorithm [32]. In such a method, the amount of required computation time grows quickly with the number of simulated particles, due to both the increase in the number of equations of motion and the more complicated force evaluations. For a polymer that is typically immersed in a solvent, a full atomistic molecular dynamics simulation of the polymer and the surrounding solvent is often not feasible. This is especially true for the escape problems, which are by nature statistical (random), and therefore several independent simulations are required to measure observables with good statistical accuracy. Therefore, in this Thesis, we make two important approximations to make the problem computationally manageable. First, we describe the polymer on a coarse-grained level as a bead-spring chain, where each bead represents several atoms of the real polymer. This approach neglects the chemical differentiation between polymer species, but is sufficient when one studies general properties, such as the dependence of the escape rate on the chain length, which apply to entire classes of polymers, instead of individual molecules. Second, we take the solvent into account only in an implicit way, by including the viscosity as a velocity-dependent frictional force, and the Brownian motion of the sol-

vent molecules as a random force. Therefore, the equations of motion for the system will be Langevin equations [cf. Eq. (1.1)] and the resulting coarse-grained description of the full dynamics is called *Langevin dynamics*.

For a polymer consisting of N beads of mass m, the Langevin dynamics description of the system has N Langevin equations of the form

$$m\ddot{\mathbf{x}}_i = -m\eta\dot{\mathbf{x}}_i - \nabla_i U_{\text{int}} - \nabla_i U_{\text{ext}} + \boldsymbol{\zeta}_i(t), \tag{2.1}$$

where $\dot{\mathbf{x}}$ indicates the derivative of $\mathbf{x}$ with respect to time and $\nabla_i \equiv \hat{x}\frac{\partial}{\partial x_i} + \hat{y}\frac{\partial}{\partial y_i} + \hat{z}\frac{\partial}{\partial z_i}$ gives the gradient w.r.t. the position of the ith monomer. The monomer-monomer interactions are described by the potential U_{int}, while U_{ext} is the external potential. The different choices of the interaction potentials U_{int} correspond to different polymer models, which will be discussed in more detail in Section 2.4. The random force $\boldsymbol{\zeta}_i$ is Gaussian white noise with zero mean, $\langle\, \boldsymbol{\zeta}_i(t)\rangle = \mathbf{0}$, and satisfies the correlations $\langle\, \boldsymbol{\zeta}_i(t) \cdot\ \boldsymbol{\zeta}_j(t')\rangle = 6k_BTm\eta\delta_{i,j}\delta(t-t')$, where η is the friction coefficient, k_B is the Boltzmann constant, T the absolute temperature, $\delta_{i,j}$ is the Kronecker delta and $\delta(t)$ is the Dirac delta function.

In the numerical implementation of Langevin dynamics, Eqs. (2.1) are discretized with time step δt and integrated numerically in time to find the positions $\mathbf{x}_i$ and the velocities $\mathbf{v}_i \equiv \dot{\mathbf{x}}_i$ of the particles as a function of time. In practice, the integration consists of setting the initial values $\mathbf{x}_i(t_0)$ and $\mathbf{v}_i(t_0)$ according to some distribution, numerically evaluating the forces due to the potentials U_{int} and U_{ext}, the friction and the random force, and then finding the positions and velocities at time $t = t_0 + \delta t$ using an appropriate algorithm. The process is then repeated using $\mathbf{x}_i(t_0+\delta t)$ and $\mathbf{v}_i(t_0+\delta t)$ as the starting values to find $\mathbf{x}_i(t_0+2\delta t)$ and $\mathbf{v}_i(t_0+2\delta t)$, and so on.

In this Thesis, two different integration algorithms have been used. The first one is the Ermak algorithm [33, 32], which employs the random force $\boldsymbol{\zeta}_i$ in a pre-integrated form as random displacement $\mathbf{x}_i^{\text{R}}$ and random velocity $\mathbf{v}_i^{\text{R}}$. The algorithm reads

$$\mathbf{x}_i(t+\delta t) = \mathbf{x}_i(t) + c_1\delta t\mathbf{v}_i(t) + c_2\delta t^2\frac{\mathbf{F}_i(t)}{m} + \mathbf{x}_i^{\text{R}} \tag{2.2}$$

$$\mathbf{v}_i(t+\delta t) = c_0\mathbf{v}_i(t) + c_1\delta t\frac{\mathbf{F}_i(t)}{m} + \mathbf{v}_i^{\text{R}}, \tag{2.3}$$

where the coefficients are $c_0 = e^{-\eta\delta t}$, $c_1 = \frac{1}{\eta\delta t}(1-c_0)$ and $c_2 = \frac{1}{\eta\delta t}(1-c_1)$ and $\mathbf{F}_i$ is the deterministic force $\mathbf{F}_i \equiv -\nabla_i(U_{\text{int}} + U_{\text{ext}})$. The random variables

$\mathbf{x}_i^{\mathrm{R}}$ and $\mathbf{v}_i^{\mathrm{R}}$ are defined as stochastic integrals

$$\mathbf{x}_i^{\mathrm{R}} = \int_t^{t+\delta t} (m\eta)^{-1} \left(1 - e^{-\eta(t+\delta t-t')}\right) \boldsymbol{\zeta}_i(t')dt' \tag{2.4}$$

$$\mathbf{v}_i^{\mathrm{R}} = \int_t^{t+\delta t} m^{-1} \left(1 - e^{-\eta(t+\delta t-t')}\right) \boldsymbol{\zeta}_i(t')dt'. \tag{2.5}$$

Since $\mathbf{x}_i^{\mathrm{R}}$ and $\mathbf{v}_i^{\mathrm{R}}$ are Gaussian random variables, they can be sampled directly from a Gaussian distribution instead of first sampling $\boldsymbol{\zeta}_i$ and then computing the integrals in Eqs. (2.4) and (2.5). The algorithm for generating the correlated Gaussian variables is described, e.g., in Ref. [32].

The second algorithm used in this thesis is the BBK (after the authors Brünger, Brooks and Karplus) algorithm, which is essentially a half-step velocity Verlet algorithm for equations of motion with explicit velocity-dependent friction [34, 35]. This algorithm updates the velocities in half time steps, while using the full time step to update the positions:

$$\mathbf{v}_i\left(t + \delta t/2\right) = \frac{\mathbf{v}_i(t)}{1 - \eta\delta t/2} + \frac{\delta t}{2}\frac{\mathbf{F}_i(t) + \boldsymbol{\zeta}_i(t)}{m} \tag{2.6}$$

$$\mathbf{x}_i\left(t + \delta t\right) = \mathbf{x}_i(t) + \delta t \mathbf{v}_i\left(t + \delta t/2\right) \tag{2.7}$$

$$\mathbf{v}_i(t + \delta t) = \frac{\mathbf{v}_i(t + \delta t/2) + \frac{\delta t}{2}\frac{\mathbf{F}_i(t+\delta t) + \boldsymbol{\zeta}_i(t+\delta t)}{m}}{1 + \eta\delta t/2}. \tag{2.8}$$

Although both algorithms are fairly robust and widely used in Langevin dynamics simulations, it turns out that implementing the Ermak algorithm with the path integral hyperdynamics (PIHD) method is problematic, while for the BBK algorithm the implementation is straightforward. This will be discussed in more detail in the following Sections.

2.2 Path integral hyperdynamics

In thermally activated barrier crossing problems, such as the Kramers escape and the corresponding problems for polymers, one typically encounters the challenge of simulating rare events. In the context of the Kramers problem, the escape from the metastable well becomes a rare event when the height of the barrier is large compared to the temperature, as we discussed in Chapter 1. In this case, the system mostly vibrates around the local energy minimum, and the time it takes for a crossing event to occur can be prohibitively long. However, since in most cases the vibrations around the energy minimum are of little interest, it would be advisable to omit the computation of those vibrations by speeding up the barrier crossing dynamics. To address this problem, the hyperdynamics method

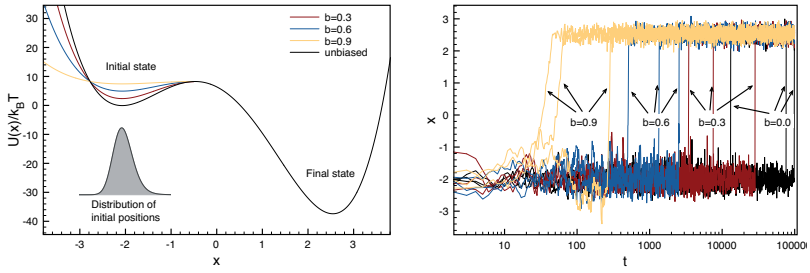

Figure 2.1. Left: a bistable potential, where the escape from the metastable initial state can be accelerated by using a bias potential. The figure shows the potential for the unbiased case and for three different biases that reduce the activation barrier by a factor of b. Right: representative trajectories in the bistable potential for different values of the bias, showing the exponential speed-up of the escape dynamics due to the reduced activation barrier.

described in Section 1.2 was introduced by Voter in 1997 [18]. However, in this Thesis, we employ a novel hyperdynamics method that is based on the path integral formulation of Langevin dynamics. The Path Integral Hyperdynamics (PIHD) method was first published by Chen and Horing [21] and subsequently also by Nummela and Andricioaei [36]. The conceptual idea of the PIHD method is similar to Voter's hyperdynamics: the residence time in the pretransition state is artificially decreased by modifying the external potential so that the activation barrier is reduced (see. Fig. 2.1). The method gives an exact correction to accelerated dynamics and is very flexible, allowing virtually any kind of potential (even time dependent) to be used as a bias. Next, before presenting a more detailed analysis of its properties, we shall derive the PIHD method starting from the path integral representation of the Langevin equation.

2.2.1 PIHD for one particle in 1D

A Brownian particle in one dimension can be approximately described with the Langevin equation

$$m\ddot{x}(t) + m\eta\dot{x}(t) - F = \zeta(t), \tag{2.9}$$

where F is the external force. The random force ζ is Gaussian with the correlations $\langle\zeta(t)\rangle = 0$ and $\langle\zeta(t)\zeta(t')\rangle = 2k_BTm\eta\delta(t-t')$, and therefore has the measure

$$P[\zeta(t)] \propto e^{-\frac{\beta}{4m\eta}\int_{t_0}^{t} dt'[\zeta(t')]^2}, \tag{2.10}$$

where $\beta = 1/k_BT$ is the inverse temperature. The path integral representation of the Langevin equation is derived by discretizing Eqs. (2.9)

and (2.10) in time, changing the variables from ζ to x, and finally going back to the continuum limit [37, 38, 39]. The resulting probability of one trajectory, or path, is, up to a normalization constant,

$$P[x(t)] = J[x]e^{-\frac{\beta}{4m\eta}\int_{t_0}^{t} dt'[m\ddot{x}(t')+m\eta\dot{x}(t')-F]^2}, \tag{2.11}$$

where $J[x]$ is the Jacobian resulting from the change of variables. For the pre-point (Itō) discretization the Jacobian can be shown to be constant and, in particular, independent of F [38, 39].

The total transition probability from $x_0 \equiv x(t_0)$ to $x_f \equiv x(t)$ is obtained by taking the path integral over all possible paths connecting x_0 to x_f, with the probabilistic weight of each path given by Eq. (2.11). For a single particle in one dimension (1D), the transition probability is then expressed as a path integral

$$P(x_f, t|x_0, t_0) = \frac{\int_{\mathcal{R}} dx'_f \delta(x'_f - x_f) \int_{x_0}^{x'_f} \mathcal{D}[x] e^{-\beta I[x(t)]}}{\int_{\mathcal{R}} dx'_f \int_{x_0}^{x'_f} \mathcal{D}[x] e^{-\beta I[x(t)]}}, \tag{2.12}$$

where $\int_{x_0}^{x'_f} \mathcal{D}[x]$ represents the path integral over all trajectories connecting (x_0, t_0) to (x'_f, t). The denominator in Eq. (2.12) ensures that the transition probability is normalized. The effective action $I[x(t)]$ is given by

$$I[x(t)] = \frac{1}{4m\eta}\int_{t_0}^{t} dt'[m\ddot{x}(t') + m\eta\dot{x}(t') - F]^2. \tag{2.13}$$

In the PIHD method, rare events such as barrier crossings are made more frequent by introducing an additional bias force $F_b(x, t)$, which is used to guide the system towards the post-transition state. In the modified system, the particle obeys the Langevin equation

$$m\ddot{x}(t) + m\eta\dot{r}(t) - F - F_b(x, t) = \zeta(t). \tag{2.14}$$

By completing the square, the action of Eq. (2.13) can be rearranged in the form $I[x(t)] = I_b[x(t)] + I_\zeta[x(t)]$, where

$$I_b[x(t)] = \frac{1}{4m\eta}\int_{t_0}^{t} dt'[m\ddot{x}(t') + m\eta\dot{x}(t') - F - F_b]^2 \tag{2.15}$$

is the action in the biased system, and

$$I_\zeta[x(t)] = \frac{1}{4m\eta}\int_{t_0}^{t} dt' F_b^2 + 2F_b[m\ddot{x}(t') + m\eta\dot{x}(t') - F - F_b] \tag{2.16}$$

is the correction due to the bias. Using Eq. (2.14), $I_\zeta[x(t)]$ can be written in a convenient form

$$I_\zeta[x(t)] = \frac{1}{4m\eta}\int_{t_0}^{t} dt' F_b(x, t')[F_b(x, t') + 2\zeta(t')], \tag{2.17}$$

where $\zeta(t)$ is the sequence of random forces in the *biased* system. By substituting $I[x(t)] = I_b[x(t)] + I_\zeta[x(t)]$ in Eq. (2.12), the transition probability in the original, unbiased system can then be expressed as

$$\begin{aligned} P(x_0, t_0|x_f, t) =& \frac{\int_{\mathcal{R}} dx'_f \delta(x'_f - x_f) \int_{x_0}^{x'_f} \mathcal{D}[x] e^{-\beta I_\zeta[x(t)]} e^{-\beta I_b[x(t)]}}{\int_{\mathcal{R}} dx'_f \int_{x_0}^{x'_f} \mathcal{D}[x] e^{-\beta I_\zeta[x(t)]} e^{-\beta I_b[x(t)]}} \\ =& \frac{\int_{\mathcal{R}} dx'_f \delta(x'_f - x_f) \int_{x_0}^{x'_f} \mathcal{D}[x] e^{-\beta I_\zeta[x(t)]} e^{-\beta I_b[x(t)]}}{\int_{\mathcal{R}} dx'_f \int_{x_0}^{x'_f} \mathcal{D}[x] e^{-\beta I_b[x(t)]}} \\ & \times \left[\frac{\int_{\mathcal{R}} dx'_f \int_{x_0}^{x'_f} \mathcal{D}[x] e^{-\beta I_\zeta[x(t)]} e^{-\beta I_b[x(t)]}}{\int_{\mathcal{R}} dx'_f \int_{x_0}^{x'_f} \mathcal{D}[x] e^{-\beta I_b[x(t)]}} \right]^{-1}. \end{aligned} \tag{2.18}$$

According to Eq. (2.18), in order to obtain the transition probability in the original, unbiased system, one may calculate the corresponding path integral in the biased system, weighted by the functional $e^{-\beta I_\zeta[x(t)]}$, which we call the PIHD *correction factor*.

In the practical implementation, it is of course not necessary to explicitly calculate the path integrals of Eq. (2.18). Since Eq. (2.14) is an equivalent description of the (biased) system, the problem reduces to calculation of weighted averages from Langevin dynamics simulations of Eq. (2.14), as is discussed in Publication I. For example, to calculate the reaction rate $\mathrm{k}_{A\to B}$ from the reactant state A to the product state B, one calculates the expectation value $\langle h_A(0) h_B(t) \rangle$ [cf. Eq (1.2)], using the accelerated dynamics of the biased system. The expectation value in the unbiased system is then recovered as

$$\langle h_A(0) h_B(t) \rangle = \frac{\langle h_A(0) h_B(t) e^{-\beta I_\xi[x(t)]} \rangle_{\mathrm{PIHD}}}{\langle e^{-\beta I_\xi[x(t)]} \rangle_{\mathrm{PIHD}}}, \tag{2.19}$$

where $\langle \cdot \rangle_{\mathrm{PIHD}}$ refers to the average computed in the biased system. Furthermore, using the Itō discretization, the integral $I_\zeta[x(t)]$ can be expressed as a discrete sum

$$I_\zeta[x(t)] = \frac{1}{4m\eta} \sum_i^{t/\delta t} F_b(x, t_i) \left[F_b(x, t_i) + 2\zeta(t_i) \right] \delta t, \tag{2.20}$$

where δt is the simulation time step.

As a last detail, we take a closer look at the normalization factor in the PIHD average, $\langle e^{-\beta I_\zeta[x(t)]} \rangle_{\mathrm{PIHD}}$. This normalization factor originates from the denominator of Eq. (2.12), which is essentially the transition probability from a pre-defined initial state to any final state. If the functional integral measure $\mathcal{D}[x]$ is properly normalized, this quantity is equal to 1. This is simple to verify. Since the random force $\zeta(t)$ in Eq. (2.17) is Gaussian with zero mean and variance given by $\langle \zeta(t) \zeta(t') \rangle = 2 k_B T m \eta \delta(t - t')$,

the functional integral $I_\zeta[x(t)]$ is itself a Gaussian random variable with mean value $\mu = \int_0^t dt' F_b(t')^2/4m\eta$ and variance $\sigma^2 = \int_0^t dt' F_b(t')^2/2m\eta\beta$. The expectation value of the correction factor is then $\langle e^{-\beta I\zeta[x(t)]}\rangle_{\mathrm{PIHD}} = e^{-\beta\mu+\beta^2\sigma^2/2} = 1$. However, the equality is exact only for an infinite number of paths. For all practical purposes, the number of sampled trajectories is finite, and therefore the relation can be only approximate,

$$\langle e^{-\beta I_\zeta[x(t)]}\rangle_{\mathrm{PIHD}} \approx 1. \tag{2.21}$$

Therefore, for consistent numerical implementation of the PIHD method, also the normalization factor should be included.

2.2.2 PIHD for a system of interacting particles

For a system of many particles, such as the polymer described by Eq. (2.1), the PIHD method can be formulated in several ways. If the position of the polymer's center of mass, $\mathbf{x}_{\mathrm{cm}} \equiv \frac{1}{N}\sum_i^N \mathbf{x}_i$, can be used as the reaction coordinate, it is possible to calculate the correction factor from the center-of-mass motion. In Publication II, where the Kramers problem for polymers is studied, this version of the PIHD method is derived. The equation of motion for the center-of-mass coordinate is

$$M\ddot{\mathbf{x}}_{\mathrm{cm}} = -M\eta\dot{\mathbf{x}}_{\mathrm{cm}} - \sum_i^N \nabla_i \left(U_{\mathrm{int}} + U_{\mathrm{ext}}\right) + \sum_i^N \boldsymbol{\zeta}_i(t), \tag{2.22}$$

where $M = Nm$ is the total mass of the polymer. The correction factor is then $e^{-\beta I_\Sigma[\mathbf{x}_{\mathrm{cm}}(t)]}$, with the correction functional

$$I_\Sigma[\mathbf{x}_{\mathrm{cm}}(t)] = \frac{1}{4M\eta}\int_{t_0}^t dt' \sum_i^N \left[\mathbf{F}_{b,i}(\mathbf{x}_i,t')\right]\cdot\left\{\sum_i^N \left[\mathbf{F}_{b,i}(\mathbf{x}_i,t') + 2\boldsymbol{\zeta}_i(t')\right]\right\}, \tag{2.23}$$

where $\mathbf{F}_{b,i}$ is the bias force for the ith particle and $\sum_i^N \mathbf{F}_{b,i}$ is the total bias force on the center of mass. However, as discussed in Publication II, the center-of-mass method only takes into account the energetic correction to the weight of the paths, being unable to correct for the entropic change in the system's free energy. Therefore, one can only apply bias forces that do not change the entropic part of the free energy, i.e., satisfy $\Delta\mathcal{F} = \sum_i^N U_b(\mathbf{x}_i)$, where $\Delta\mathcal{F}$ is the free-energy difference between the biased and unbiased states, and U_b is the bias potential. It can be shown that a constant-force bias $\mathbf{F}_{b,i}(\mathbf{x}_i,t) = \mathbf{F}_b$ satisfies this criterion. However, the restriction to constant-force biasing is very limiting, and therefore a

different formulation of the PIHD method for polymer systems is desirable.

It turns out that the the center-of-mass method with the constant-force bias is a special case of a more general formulation of PIHD. Similarly to the one degree of freedom, the probability of a given trajectory for the $3N$ degrees of freedom of the polymer is given by

$$P[\boldsymbol{\zeta}_1(t),\ldots,\boldsymbol{\zeta}_N(t)] = P[\boldsymbol{\zeta}_1(t)]\cdots P[\boldsymbol{\zeta}_N(t)] \propto e^{-\frac{\beta}{4m\gamma}\int_{t_0}^{t} dt' \sum_i^N [\boldsymbol{\zeta}_i(t')]^2}, \quad (2.24)$$

where we have used the fact that the random forces for the different degrees of freedom are uncorrelated. A change of variables gives, analogously to Eq. (2.11),

$$\begin{aligned} &P[\mathbf{x}(t)_1,\ldots,\mathbf{x}_N(t)] = \\ &\qquad J[\mathbf{x}_1]\cdots J[\mathbf{x}_N] e^{-\frac{\beta}{4m\eta}\int_{t_0}^{t} dt' \sum_i^N [m\ddot{\mathbf{x}}_i(t')+m\eta\dot{\mathbf{x}}_i(t')+\nabla_i(U_{\rm int}+U_{\rm ext})]^2}. \end{aligned} \quad (2.25)$$

As in the 1D case, the Jacobians $J[\mathbf{x}_i]$ can be shown to be constant under the Itō discretization. Henceforth, the derivation goes exactly as in the 1D case. In the biased system, the system obeys the equations of motion

$$m\ddot{\mathbf{x}}_i = -m\eta\dot{\mathbf{x}}_i - \nabla_i(U_{\rm int}+U_{\rm ext}) - \nabla_i U_b + \boldsymbol{\zeta}_i(t). \quad (2.26)$$

The $3N$-dimensional correction functional is then, according to Eq. (2.25), the sum of single particle 1D correction functionals:

$$\begin{aligned} &I_\Sigma[\mathbf{x}_1(t),\ldots,\mathbf{x}_N(t)] = \\ &\qquad \frac{1}{4m\eta}\int_{t_0}^{t} dt' \sum_i^N \left\{\mathbf{F}_{b,i}(\mathbf{x}_i,t')\cdot[\mathbf{F}_{b,i}(\mathbf{x}_i,t')+2\boldsymbol{\zeta}_i(t')]\right\}. \end{aligned} \quad (2.27)$$

The correction factor is then given as $e^{-\beta I_\Sigma[\mathbf{x}_1(t),\ldots,\mathbf{x}_N(t)]}$, similar to the single particle in 1D.

If the bias force is independent of x and is the same for all monomers, $\mathbf{F}_{b,i}(\mathbf{x}_i,t) = \mathbf{F}_b(t)$, the expressions (2.23) and (2.27) are equal. Therefore, in the center-of-mass description the correction factor is calculated correctly if the bias force is the same for each monomer, although it may change in time. However, using the $3N$-dimensional correction functional of Eq. (2.27), the bias force can be position or time dependent, and may even be different for different particles. Therefore, this latter form retains the flexibility of the original one degree-of-freedom PIHD.

2.3 Efficiency of the PIHD method

The primary application of the path integral hyperdynamics method is the acceleration of rare event computation by reducing the activation barrier.

Therefore it is interesting to study the efficiency of the method compared to unbiased molecular (Langevin) dynamics simulations. In Publication I, we have studied the efficiency of the PIHD method by looking at the benchmark example of monomer diffusion on a 1D periodic potential. The system obeys the Langevin equation (2.9), with the external force given by $F(x) = \frac{\pi V_B}{\lambda} \sin\left(\frac{2\pi}{\lambda}x\right)$, where V_B is the barrier height and λ is the lattice spacing. For sufficiently low temperatures ($k_B T \ll V_B$), the diffusion occurs in discrete jumps between the neighboring minima, and the calculation of the diffusion coefficient reduces to finding the crossing rate from one minimum to the next [40].

To quantify the efficiency of the PIHD method, in Publication I we have studied the *boost factor* B, defined as the ratio of computational time of conventional MD (Langevin) simulations over the computational time of PIHD simulations required to give the same accuracy of the crossing rate. In practice, since it is difficult to know the statistical error of the crossing rate *a priori*, the boost factor is measured by running the same number of trajectories in the biased and unbiased systems and determining the mean squared error (MSE) separately for both cases. The boost factor is then given as the ratio

$$B = \mathrm{MSE}_{\mathrm{MD}}/\mathrm{MSE}_{\mathrm{PIHD}}, \tag{2.28}$$

with the smaller error from the PIHD simulations giving a boost factor $B > 1$.

The boost factor was measured for two different types of bias forces with several magnitudes to demonstrate the dependence of the PIHD efficiency on the employed bias force. The two bias forces were the constant bias force, defined as $F_b(x) = f_b$ for $x < \lambda/2$ and 0 for $x \geq \lambda/2$, and the sinusoidal bias force, defined as $F_b(x) = -\frac{\pi V_b}{\lambda}\sin(2\pi x/\lambda)$, for $-\lambda/2 \leq x \leq \lambda/2$, and 0 otherwise. The crossing probabilities and the corresponding jump rates (analogous to the forward crossing rates $\mathrm{k}_{A\to B}$ discussed earlier in this Thesis) are shown in Figures 2.2 and 2.3. Due to the reduced barrier, the number of successful crossings given by the PIHD simulations is orders of magnitude larger than for the unbiased MD simulations, resulting in much smoother $p(t)$ curves. The error estimate for the jump rate is correspondingly improved. However, especially for the constant bias force (Figure 2.2), large bias forces induce a significant systematic error, which leads to underestimated jump rates. This systematic error is due to inefficient sampling of the most relevant transition paths, which may occur when the bias severely changes the original system.

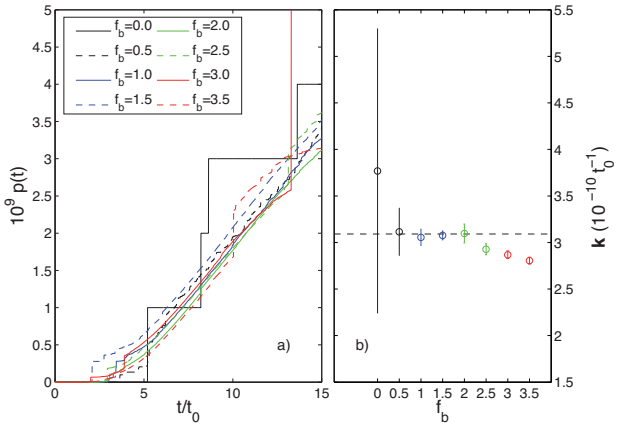

Figure 2.2. (a) The crossing probability $p(t)$ *vs.* time t of a Brownian monomer in a sinusoidal potential well with $V_B/T = 20$. The regular MD simulations yield only four crossings out of 10^9 runs, while the PIHD simulations give several orders of magnitude more. (b) The jump rate $\mathrm{k} = \frac{dp(t)}{dt}$ for bias force values $f_b = 0\ (\mathrm{MD}), 0.5, 1.0, 1.5, 2.0, 2.5, 3.0, 3.5$. The error bars indicate the standard error of the mean value. The dashed horizontal line indicates the theoretical value at the low temperature and high friction limit, $\mathrm{k} \approx 3.0919 \cdot 10^{-10}$. The time is expressed in units of $t_0 = \lambda\sqrt{m/k_B T}$.

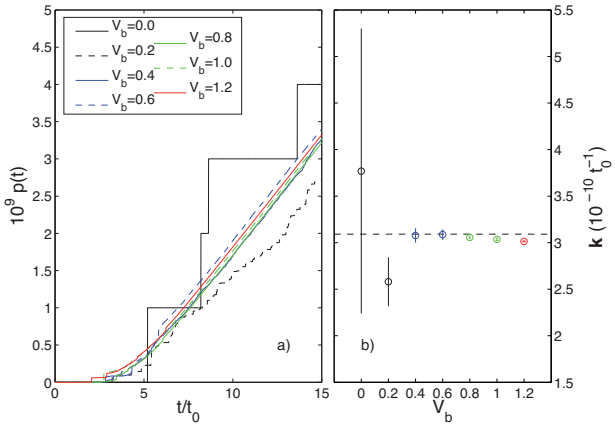

Figure 2.3. The crossing probability (panel a) and jump rate (panel b) for the sinusoidal bias force with $V_b = 0, 0.2, 0.4, 0.6, 0.8, 1.0, 1.2$. Conventions are the same as in Fig. 2.2.

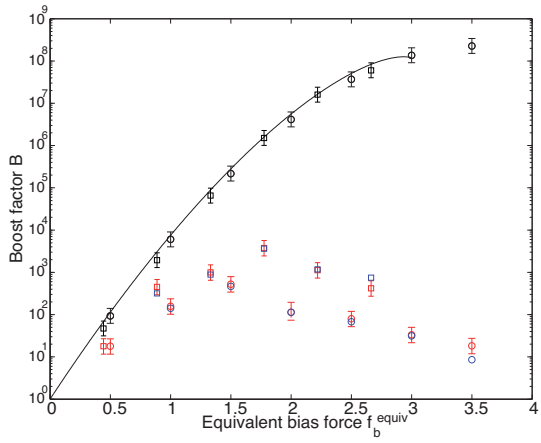

Figure 2.4. The PIHD boost factor B as a function of equivalent constant bias force f_b^{equiv} for both the constant bias force (circles) and the sinusoidal force (squares). For the constant bias force, $f_b^{\mathrm{equiv}} = f_b$, while for the sinusoidal force, $f_b^{\mathrm{equiv}} = \frac{\pi}{\sqrt{2}} V_b$. The solid black curve indicates the theoretical gain in number of crossings, with the black markers being the corresponding values from PIHD simulations. The red markers with error bars are the boost factors measured from simulations. The blue markers show the corresponding values calculated with a theoretical model (see Publication I).

Inefficient sampling also reduces the boost factor B. As shown in Figure 2.4, the number of crossings increases roughly exponentially with increasing bias force. Although the boost factor reaches a respectable value of $B \approx 4000$, it grows substantially slower than the number of crossings, and even decreases for very large bias forces. This is because the PIHD average, Eq. (2.19), is dominated by the trajectories that give small values of the correction integral $I_\zeta[x(t)]$, Eq. (2.17). Because $I_\zeta[x(t)]$ is approximately a Gaussian random variable with mean $\mu = \int_0^t dt' F_b(t')^2/4m\eta$ and variance $\sigma^2 = \int_0^t dt' F_b(t')^2/2m\eta\beta$, the probability to find small values of $I_\zeta[x(t)]$ decreases with increasing bias. This is illustrated in Figure 2.5, where the probability distribution $P(I_\zeta)$ for trajectories crossing the barrier is given. Clearly, as the number of crossing paths increases, the relative number of paths with significant probabilistic weight decreases. The boost factor B is therefore a product of two competing factors: the increasing number of crossing paths, and the diminishing contribution of those paths. This competition leads to the boost factor having a maximum at a finite bias. Thus, the efficiency of the PIHD method cannot be increased without limit. Rather, there exists an optimal strength of the bias, which gives the best performance. Qualitatively, the optimal bias should be strong enough to significantly speed up the barrier crossing, but also modest enough to preserve the essential features and symme-

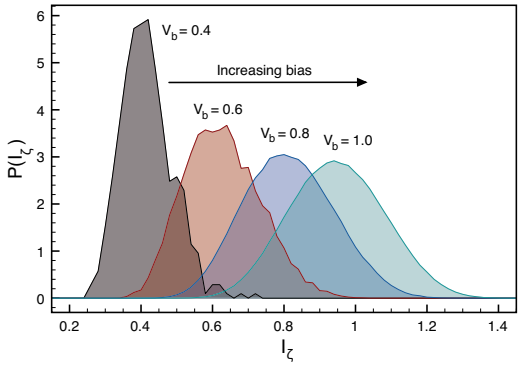

Figure 2.5. The distribution $P(I_\zeta)$ of the correction integral I_ζ at the moment of barrier crossing for the sinusoidal bias potential with $V_b = 0.4, 0.6, 0.8, 1.0$. The distribution is calculated from crossing events occurring between $9 \leq t/t_0 \leq 10$.

tries of the system. For instance, the sinusoidal bias potential starts to lose its effectiveness when the bias is so strong that the activation barrier disappears altogether.

With the PIHD method, there is also an additional concern with respect to the choice of the numerical integrator. The simulations in Publication I were performed with both the Ermak algorithm and the BBK algorithm described in Section 2.1. For similar accuracy, the Ermak integrator required an approximately ten times shorter time step for the PIHD simulations, while with the BBK integrator the same time step could be used for both MD and PIHD runs. The reason for this is that in the Ermak integrator, the random force appears in the algorithm in a pre-integrated form, which is not fully compatible with PIHD. The value of the correction factor is extremely sensitive to the value of the random force in $I_\zeta[x(t)]$, and therefore the Ermak scheme introduces a subtle error in the estimation of the correction factor. With the BBK integrator this problem does not occur.

In Publication I, also a different way to implement PIHD for computational gain was studied. Since any external bias force can be used, it is possible to resample the results from one PIHD run to several different bias values, thereby obtaining the results for many different systems at once. This *parallel resampling* was implemented for the problem of a monomer diffusing in a 1D periodic potential with an additional time-dependent sinusoidal driving force of the form $A\sin(2\pi\nu t)$, where ν is the driving frequency and A is the amplitude. The PIHD simulation was run with $A = 0$ and the results from that one simulation were resampled to 100 different combinations of (A, ν). Compared to MD simulations run

separately for each combination of (A, ν), the PIHD attained a modest boost of $B \approx 2 - 3$. This is because the equation of motion was so simple that most of the computation time was spent in calculating the correction integrals $I_\zeta[x(t), A, \nu]$ for the different A and ν. Arguably, for more complicated system, the boost could be significantly higher, because the computational complexity of $I_\zeta[x(t)]$ does not necessarily increase with the complexity of the equations of motion. Therefore, applied to a more complicated system, also the parallel resampling has the potential to provide a significant computational boost.

Finally, we take a look at the normalization factor $\langle e^{-\beta I_\zeta[x(t)]} \rangle$. As we discussed earlier, the normalization factor is in principle equal to $\langle e^{-\beta I[x(t)]} \rangle = 1$ for infinite number of paths. However, since the number of paths in a simulation is never infinite, the normalization factor depends on the realizations of the sampled paths and, through that, also on time. Because the standard deviation of the correction integral grows with time, also the normalization factor becomes noisier for large t. This behavior is shown in Figs. 2.6 and 2.7, where the crossing probabilities and normalization factors are shown for the sinusoidal bias force ($V_b = 1.0$) and for the constant bias force ($f_b = 2.0$), respectively. For the sinusoidal force, although the normalization factor starts to deviate from unity as time progresses, the difference is less than 0.05 %. Correspondingly, the unnormalized crossing probability (calculated with the assumption $\langle e^{-\beta I[x(t)]} \rangle = 1$) and the normalized crossing probability (calculated with the time-dependent normalization factor) are almost equal. On the other hand, for the constant bias force, the normalization factor is significantly noisier, due to the inefficient sampling of the high-probability trajectories. Consequently, the normalized crossing probability becomes extremely noisy for long simulation times. The unnormalized curve remains very smooth, but bends down due to the missing normalization of the probability.

In Publications I and II, the approximation of $\langle e^{-\beta I[x(t)]} \rangle = 1$ was used for the normalization factor. Although this is strictly speaking valid only for infinite number of trajectories, in practice it is a very good approximation for most cases. Typically, and also in Publications I and II, the crossing rate is measured from the linear part of the $p(t)$ curve. The unnormalized probability curve is linear only when the normalization factor is unity with good accuracy, and therefore, in practice, the unnormalized $p(t)$ is no different from the normalized one. However, keeping track of the normalization factor and calculating the normalized quantities makes it

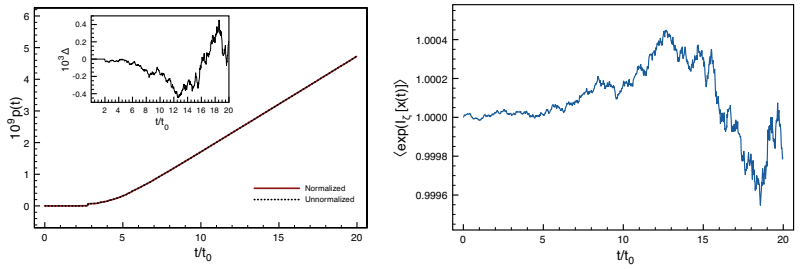

Figure 2.6. Left: the normalized (p_{n}) and unnormalized (p_{u}) crossing probability as a function of time for the sinusoidal bias force with $V_b = 1.0$. The inset shows the normalized difference between the probabilities: $\Delta = (p_{\mathrm{n}} - p_{\mathrm{u}})/p_{\mathrm{u}}$. Right: the normalization factor as a function of time.

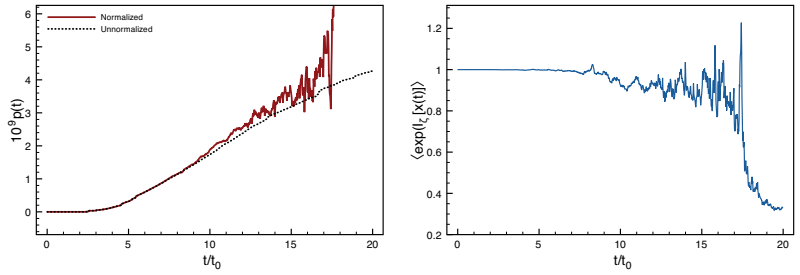

Figure 2.7. Left: the normalized and unnormalized crossing probability as a function of time for the constant bias force with $f_b = 2.0$. Right: the normalization factor as a function of time.

somewhat easier to recognize when the applied bias is inefficient. For instance, the normalization factor for the linear bias becomes very noisy even for moderate bias forces f_b, while for the sinusoidal force the normalization factor remains very close to 1 even for large values of V_b. This is another indication towards the better efficiency of the sinusoidal bias.

2.4 Kramers escape problem for polymers

The essential difference between the one dimensional single particle problem considered originally by Kramers [14] and the corresponding problem for polymers, is the internal degrees of freedom of the polymer chain. A polymer chain can change its shape by coiling, swelling and stretching. The chain flexibility adds an important entropic contribution to the free energy, and can significantly alter the effective free-energy barrier [25]. For the ideal chain, depending on the size of the polymer in relation to the dimensions of the external potential, several different regimes can be identified. When the contour length of the chain is small compared to the width of the well and the barrier, one can analyze the problem with a many-body generalization of the Kramers problem and use the saddle-point approximation to calculate the crossing rate, e.g., as a function of chain length [25]. In this regime, the flexibility of the chain enables the so-called coil-to-stretch transition. Here the polymer, initially in a coiled configuration at the bottom of the well, assumes a highly elongated conformation at the barrier top. Because of this, the free-energy barrier is lower and the crossing rate significantly higher than in the globular limit ($k \to \infty$, $l_0 \to 0$). After a certain critical chain length, the rate even starts to increase as a function of chain length.

In the opposite limit, where the contour length of the chain is much larger than the width of the well, the chain is able to occupy both the well and barrier regions at the same time. It has been suggested that in this limit the motion of the chain is described by an excitation and motion of a kink-antikink pair [28]. According to this description, the motion of the kink occurs at constant velocity, leading to an inverse dependence of the crossing rate on the chain length. In the intermediate regime, depending on the exact parameters, the crossing rate may have a minimum at certain chain length due to the confinement of the chain in the well [25, 29], although the rate eventually approaches the long chain limit.

For the realistic polymer, also the excluded volume interactions and fi-

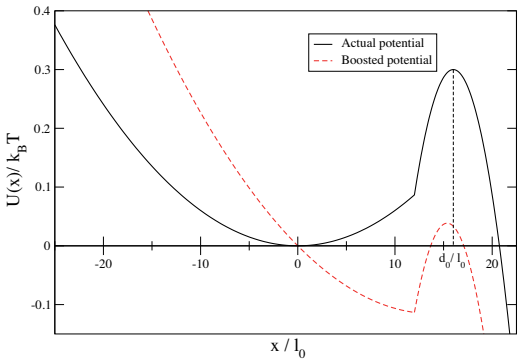

Figure 2.8. The original potential (black solid line) and the biased potential (red dashed line) used in Publication II. In the direction perpendicular to the x axis, the potential is constant.

nite chain flexibility are expected to influence the crossing rate [27]. In Publication II, we have studied the polymer escape dynamics with PIHD simulations in the intermediate chain length regime, where the non-ideal polymer interactions may cause significant differences between the polymer models. In this numerical implementation, the polymer is described by the Langevin Eqs. (2.1), with the interaction potential $U_{\rm int}$ depending on the type of polymer. For the ideal polymer, one can use a simple potential with harmonic interactions between the consecutive monomers:

$$U_{\rm harm} = \sum_{i=1}^{N-1} \frac{1}{2} k \left(|\mathbf{x}_i - \mathbf{x}_{i+1}| - l_0 \right)^2 , \tag{2.29}$$

where k is the spring constant and l_0 is the zero-temperature equilibrium separation. The finite flexibility of the polymer can be modeled by including an additional bending energy term. Then, the interaction potential is given by $U_{\rm int} = U_{\rm harm} + U_{\rm bend}$, with the bending energy $U_{\rm bend}$ defined as

$$U_{\rm bend} = \sum_{i=2}^{N-1} \frac{1}{2} \kappa \left(\mathbf{x}_{i-1} - 2\mathbf{x}_i + \mathbf{x}_{i+1} \right)^2 . \tag{2.30}$$

Here κ is the bending stiffness of the semi-flexible polymer. The flexible ideal chain limit is given by $\kappa = 0$.

For the self-avoiding polymer, one typically considers the bonds between the consecutive monomers and the excluded volume interactions separately. A widely used model is the self-avoiding FENE (finitely extensible nonlinear elastic) chain, where the interaction potential is given by a combination of FENE springs and short-range repulsive Lennard-Jones (LJ) interactions: $U_{\rm int} = U_{\rm FENE} + U_{\rm LJ}$. The FENE potential is defined as

$$U_{\rm FENE} = -\sum_{i=1}^{N-1} \frac{1}{2} k_{\rm F} R_0^2 \ln \left(1 - \left(\mathbf{x}_i - \mathbf{x}_{i+1} \right)^2 / R_0^2 \right) , \tag{2.31}$$

where k_{F} is the FENE spring constant and R_0 is the maximum allowed separation between connected monomers. The LJ potential is

$$U_{\mathrm{LJ}} = \sum_{i<j}^{N} 4\epsilon \left[(\sigma/r_{ij})^{12} - (\sigma/r_{ij})^{6} \right] + \epsilon, \tag{2.32}$$

for $r_{ij} \leq 2^{1/6}\sigma$ and 0 for $r_{ij} > 2^{1/6}\sigma$. Here $r_{ij} = |\mathbf{x}_i - \mathbf{x}_j|$ is the separation of the monomers, σ is the diameter of the monomer and ϵ controls the steepness of the potential.

The three chain models were studied in a metastable external potential similar to the original Kramers problem (see Figure 2.8). The study was performed in two dimensions to contrast the differences between the ideal and self-avoiding chains due to the excluded volume interactions. The main results of the study are shown in Figure 2.9. For the flexible ideal chain, the crossing rate k steadily decreases with chain length N, although the rate is consistently higher than in the globular limit. This agrees with the theoretical prediction of Ref. [29]. Adding either the bending energy or the excluded volume interaction has a similar effect on the dynamics. In both cases, the crossing rate for long chains is significantly higher than for the flexible chain, and the self-avoiding chain even has a minimum in the crossing rate, with long chain crossing faster than intermediate chains. The fundamental reason for the higher crossing rate is the same for both the semi-flexible and the self-avoiding chain. Because of the additional interactions, the chains tends to swell and occupy a larger volume. Due to the confining external potential, the swelling is partially prohibited, leading to an increased free energy especially at the bottom of the metastable well. In addition, due to the larger radius of gyration of the polymer, also the states at the barrier top typically are more extended than for the flexible chain, and therefore at lower energy. Consequently, the free energy barrier for the semi-flexible and self-avoiding chains has a maximum at certain chain length, whereas for the flexible chain this does not occur (see Figure 2.10). This fact accentuates the importance of considering more realistic chain models in addition to the theoretically tractable ideal chain models. In addition, the results suggest interesting possibilities for polymer separation with respect to, e.g., chain length and bending stiffness.

As was discussed in Section 2.2, in Publication II the center-of-mass PIHD was used to accelerate the crossing dynamics. The estimated speed-up for the flexible ideal chain was of the order of 30. For the self-avoiding chain the boost was slightly smaller due to the relatively high crossing

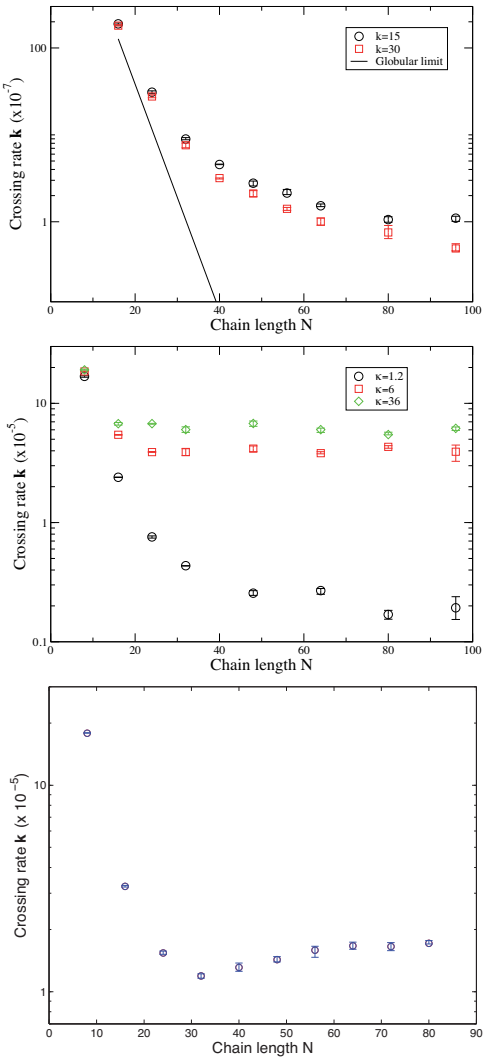

Figure 2.9. The crossing rate k as a function of chain length N for the ideal (top panel), semiflexible (middle panel) and self-avoiding polymer (bottom panel). For the ideal chain, data is shown for two different spring constants, $k = 15$ and $k = 30$, while for the semi flexible chain, data is shown for the bending stiffnesses $\kappa = 1.2$, $\kappa = 6$ and $\kappa = 36$.The solid line in the top panel shows the crossing rate in the globular limit.

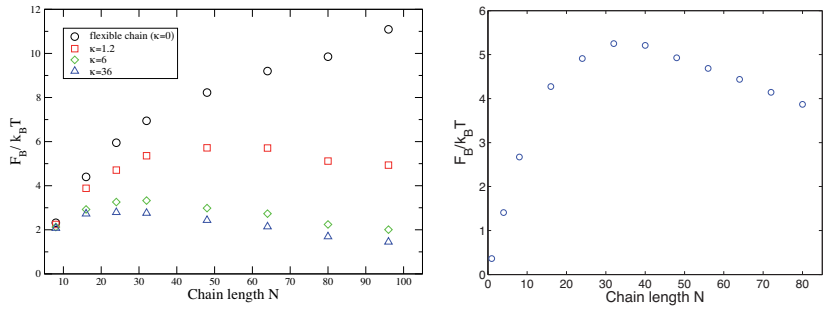

Figure 2.10. The free-energy barrier height F_B as a function of chain length for the flexible and semi-flexible chain (left) and the self-avoiding chain (right). The crossing rates shown in Figure 2.9 roughly correspond to k $\propto \exp\left[-F_B(N)/k_BT\right]$.

rate and weaker separation of barrier crossing and intrawell vibration time scales. While the center-of-mass formulation of the method fits the polymer escape problem very well, in principle it limits the available choices of the bias potential. In a later work, the PIHD method was employed in the alternative form, where the correction factor is calculated from all the $3N$ degrees of freedom [41]. In this form of PIHD, any form of the bias potential can be used – even applying the bias force only on some of the particles is possible. However, the study indicated that the original way of applying the same bias force on all the particles was the most efficient one among the tested biasing scenarios.

3. Polymer translocation

3.1 Polymer translocation under static force

3.1.1 Review of theories of driven translocation

The first attempts to model polymer translocation theoretically were made by Sung and Park [42] and later by Muthukumar [43]. In their approach, driven translocation was viewed as a one-dimensional barrier crossing problem of the translocation coordinate s (the length of the subchain on the *trans* side), with the dynamics of the system determined by the system's free energy $\mathcal{F}$. In this description, the chain starts from the *cis* side with one end inside the pore ($s = 0$) and is considered as translocated once $s = aN$, with a the segment length. The free-energy $\mathcal{F}$ due to chain entropy and the chemical potential difference $\Delta\mu$ is

$$\mathcal{F}(s) = (1-\gamma')k_BT \ln\left[\frac{s}{a}\left(N - \frac{s}{a}\right)\right] + \frac{s}{a}\Delta\mu, \tag{3.1}$$

where γ' is the surface exponent ($\gamma' = 0.5, \approx 0.69, \approx 0.95$ for an ideal chain, and a self-avoiding chain in 2D and 3D, respectively). The problem can then be solved with standard methods by deriving, e.g., the corresponding Langevin equation or the Fokker-Planck equation for s [42], or by using nucleation theory [43]. The central result is the dependence of the mean translocation time τ on the chain length N. This is typically characterized by the scaling exponent α, defined as $\tau \sim N^\alpha$. The barrier crossing model predicts that $\tau \sim \Gamma N$, where Γ is the effective friction for the system. Sung and Park considered the friction to be due to the Rouse type dynamics of the whole chain, giving $\Gamma \sim N$, while Muthukumar argued that the friction is due to the interactions between the polymer and the pore, leading to $\Gamma \sim 1$. Therefore, the barrier crossing model for poly-

mer translocation predicts the scaling between $\alpha = 1$ and $\alpha = 2$, depending on whether the dominant friction in the system is the polymer-pore friction or the polymer-solvent friction. The polymer-pore friction dominated case was also considered by Lubensky and Nelson, who described the translocation of the polymer through the pore as diffusion in a tilted one-dimensional periodic potential [44].

Several theoretical and simulation studies have shown, that within the relevant range of driving forces, the polymer chain is in fact rarely in equilibrium [45, 46, 47, 48, 49, 50, 51]. As argued by Chuang, Kantor and Kardar [45, 46], an asymptotic lower bound for the scaling exponent α is given by the transport of the polymer without the hindrance of the wall. A polymer of length N occupies a volume comparable to its radius of gyration, $R_g \sim N^\nu$, where ν is the Flory exponent ($\nu = 0.5, \ \approx 0.588, \ = 0.75$ for an ideal chain, and a self-avoiding chain in 2D and 3D, respectively). The distance the polymer has to traverse when crossing from the *cis* side to the *trans* side is comparable to its size, and therefore the translocation time is $\tau \sim \Gamma N^\nu \sim N^{1+\nu}$. Later, Vocks *et al.* suggested another scaling law, $\tau \sim N^{\frac{1+2\nu}{1+\nu}}$, based on memory effects due to tension imbalance between the *cis* and *trans* sides in the vicinity of the pore [52]. Also Dubbeldam *et al.* derived a different value, $\tau \sim N^{2\nu+1-\gamma'}$, using scaling arguments based on the assumption of partial equilibrium of the chain [53]. Using the obtained α, they further analyzed the dynamics with the fractional Fokker-Planck formalism, first employed in the context of polymer translocation by Metzler and Klafter [54].

Recently, Sakaue introduced a novel theoretical formalism, where the non-equilibrium nature of the process is inherently taken into account [55, 56, 57, 58]. In this formalism, translocation is described as a two-stage process, where the drag force due to the *cis* side subchain changes in time. In the first stage, the drag force increases as the chain is gradually set in motion by non-equilibrium tension propagation and, in the last stage, the drag force decreases due to the *cis* side subchain getting shorter as it is sucked into the pore by the driving force. This tension propagation mechanism leads to extremely nontrivial dynamics, which Sakaue analyzed in the infinite chain length limit. For asymptotically long chains, Sakaue derives the scaling of translocation time as $\tau \sim N^{\frac{1+\nu+2\nu^2}{1+\nu}}$ for driving forces between $k_B T N^{-\nu} \lesssim f \lesssim k_B T N^\nu$, and $\tau \sim N^{1+\nu}$ otherwise. Later it was argued by Rowghanian & Grosberg [59], Dubbeldam et al. [60] and by the author of this Thesis in Publication III, that the result in the intermediate

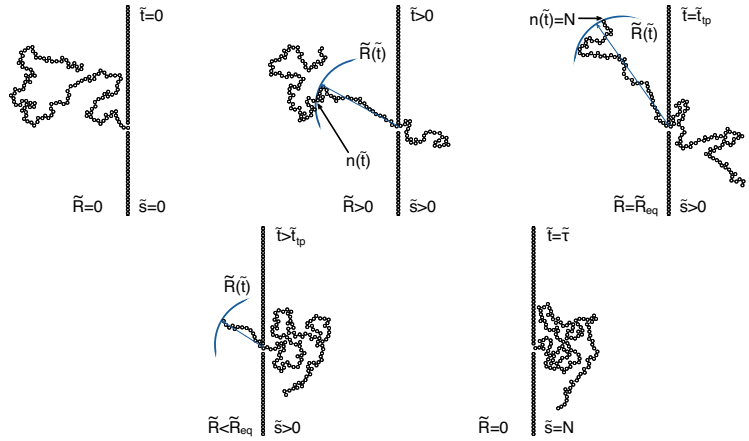

Figure 3.1. The time evolution of the polymer configuration during the translocation process, with time advancing from left to right, top row preceding the bottom row. The arc denotes the position of the tension front $\tilde{R}$, which separates the chain into the moving and nonmoving domains. The last monomer inside the front is denoted by N and the number of translocated monomers by $\tilde{s}$. The rightmost panel on the top row corresponds to the end of the tension propagation stage.

regime is in fact caused by a violation of mass conservation, and that the correct scaling behavior also in that regime is $\tau \sim N^{1+\nu}$. This result also matches with the lower bound proposed by Kantor and Kardar [46].

Molecular dynamics simulations of polymer translocation have shown that dynamical scaling exponents, such as α, depend on several system parameters, including temperature, solvent friction, chain length, driving force and pore size [61, 64, 63, 65, 49]. However, all previous theories assume the universality of the scaling exponents, which in light of the numerical simulations, is not true. As a result, previous theoretical endeavors have succeeded in reproducing only some of the measured numerical values of α, and typically not with very good accuracy. In particular, no theory has been able to reproduce all the simulation results in different regimes. In fact, even very recently some authors considered such a goal unachievable [59]. However, as a part of this Thesis, a very general model of driven translocation is presented. In Publication III, we show that the tension propagation formalism can indeed explain all previous MD simulation results, but only if finite chain length effects are taken into account. Furthermore, in Publication IV, the role of these finite chain length effects is examined in more detail.

3.1.2 Tension propagation theory of polymer translocation

In Publications III & IV, the tension propagation formalism is employed in a new context. The starting point is the free energy of Eq. (3.1), from which the Brownian equation of motion for the translocation coordinate $s(t)$ can be derived,

$$\Gamma(t)\frac{ds}{dt} = (1-\gamma')k_BT\left[\frac{1}{aN-s} - \frac{1}{s}\right] + f + \zeta(t) \equiv f_{\rm tot}. \qquad (3.2)$$

As discussed in the previous Section, Sung & Park considered the case $\Gamma \sim N$, while in Muthukumar's theory, $\Gamma \sim 1$. Notably, in both cases, the effective friction Γ is independent of time. However, for the non-equilibrium problem of driven translocation, neither of these choices is realistic. Typically, for driven translocation the translocation time τ is much smaller than the chain relaxation time. Therefore, for most of the process, the chain is out of equilibrium and responds to the driving force not as a whole, but by starting to move in stages. As will be argued below, this leads to time-dependence of the effective friction, $\Gamma = \Gamma(t)$. In Publications III & IV, the Brownian equation is combined with a modified tension propagation formalism to give the so-called BDTP model of driven polymer translocation. Within this model, the effective friction $\Gamma(t)$ is given by the tension propagation equations, while the Brownian equation of motion provides a framework for measuring various quantities of the translocation process.

The central idea of the tension propagation (TP) formalism is to divide the subchain on the *cis* side into two distinct domains [55, 58, 56, 57]. The first domain, closer to the pore, consists of all the monomers that are pulled towards the pore by the external driving force. The second domain consists of the remaining monomers, which are at rest (on the average). As the driving force is applied at the pore, the chain begins to move in stages, with the segments closest to the pore being set into motion first. A close analogue is a coil of rope pulled from one end, which first has to uncoil and become tense before starting to move as a whole. To keep track of the moving part of the chain, one defines a *tension front*, which divides the chain into the moving and nonmoving domains. The front propagates in time as parts of the chain further away from the pore are set in motion, as shown in Fig. 3.1. As the monomers enter the front and start to move, the effective friction Γ increases due to the increased drag between the polymer and the solvent. After a certain tension propagation time, $t_{\rm tp}$, the front reaches the end of the chain and the tension propagation

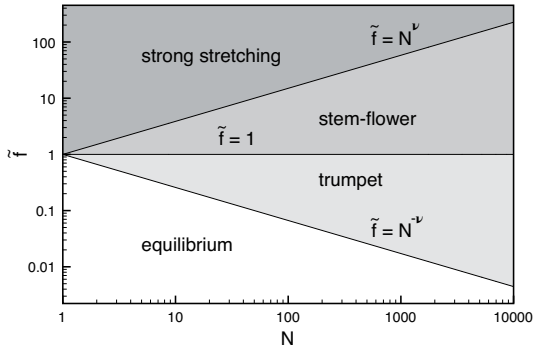

Figure 3.2. The different scaling regimes of driven polymer translocation. For extremely small forces, the chain is in equilibrium, responding to the driving force as a whole, while for very strong forces, the moving part of the *cis* side chain is stretched almost completely straight. In the intermediate regimes, the moving part of the chain follows the Pincus blob description, with the size of the blobs increasing as one moves further away from the pore.

process stops. After this time, the chain as a whole is pulled towards the pore. During this stage, the overall length of the subchain on the *cis* side decreases, which reduces the effective friction Γ. This stage continues until the last monomer reaches the pore and finally translocates at time $t = \tau$.

The effective friction $\Gamma(t)$ actually consists of two contributions. The first one is the drag force of the *cis* side subchain that is solved with the TP formalism. The other one is the frictional interaction between the pore and the polymer. Formally, we can write Γ as the sum of the *cis* side subchain and pore frictions, $\Gamma(t) = \eta_{\mathrm{cis}}(t) + \eta_p$. While for $N \to \infty$ the first term dominates, for finite N the pore friction can significantly affect the translocation dynamics. Since the pore friction η_p characterizes the totality of frictional interactions between the pore and the polymer, it depends on several local and system-specific factors such as pore diameter and length, cross-sectional shape, pore material, etc. Therefore, it seems at present impossible to derive the exact value of η_p for each pore type from microscopic theory. Instead, the pore friction can be measured from experiments or simulations by comparing, e.g., the monomer waiting time distribution. This quantity essentially tells the time it takes for the individual monomer to traverse from one end of the pore to the other. This time of course depends on the friction between the pore and the monomer, giving a convenient way to determine η_p. In Publication IV, the dependence of η_p on the pore geometry is studied further.

The derivation of the tension propagation equations is presented in Pub-

lication III and is not repeated here. We merely note that the TP formalism can be used to derive an equation of motion for the tension front, using either the location of the front R or the index of the last monomer inside the front, n, as the dynamical variable. The choice of the variable depends on the dynamical scaling regime that is determined by the magnitude of the driving force. Before describing the different scaling regimes, we introduce the dimensionless units denoted by the tilde symbol as $\tilde{X} \equiv X/X_u$, with the unit of length $a_u \equiv a$, force $f_u \equiv k_B T/a$, time $t_u \equiv \eta a^2/k_B T$, velocity $v_u \equiv a/t_u$ and friction $\eta_u \equiv \eta$, where η is the solvent friction per monomer.

The simplest case is the *strong stretching* (SS) regime that is realized when the driving force is very large compared to temperature and chain length, $\tilde{f} \gtrsim N^\nu$ (see Figure 3.2). In this regime, the moving part of the chain is almost completely straight. The equation of motion is most conveniently derived for n, giving

$$\frac{dn}{d\tilde{t}} = \frac{\tilde{f}_{\rm tot}}{\tilde{\Gamma}(\tilde{t})\,(1-\nu A_\nu n^{\nu-1})}. \tag{3.3}$$

Here, $\tilde{\Gamma}(\tilde{t}) = n(\tilde{t}) - \tilde{s}(\tilde{t}) + \tilde{\eta}_p$, with $n(\tilde{t}) - \tilde{s}(\tilde{t})$ being the number of moving monomers on the *cis* side. The Flory exponent ν and the prefactor A_ν are related to the end-to-end distance of the polymer, $\tilde{R}_{\rm ee} = A_\nu N^\nu$.

For slightly smaller driving forces, $1 \lesssim \tilde{f} \lesssim N^\nu$, the force is not sufficient to completely straighten the chain. Due to thermal fluctuations, a flower-shaped tail develops (see Fig. 3.1). In this *stem-flower* (SF) regime, the line density and velocity of the monomers are not constant in space. Therefore, one also has to solve the density $\tilde{\sigma}_R$ and the velocity $\tilde{v}_R$ near the tension front. As a result, one gets a system of equations,

$$\frac{d\tilde{R}}{d\tilde{t}} = \tilde{v}_R \left[\frac{1}{\nu} A_\nu^{-1/\nu} \tilde{\sigma}_R^{-1} \tilde{R}^{1/\nu-1}\right]^{-1}, \tag{3.4}$$

$$\tilde{\sigma}_R^{1/(\nu-1)} = \frac{\tilde{v}_0 \tilde{R}}{\nu b \tanh(b)} \ln\left[\cosh\left(b \frac{\tilde{\sigma}_R^{\nu/(1-\nu)}}{\tilde{R}}\right)\right], \tag{3.5}$$

$$\tilde{v}_R = \tilde{v}_0 \frac{\tanh\left(b\tilde{\sigma}_R^{\nu/(1-\nu)}/\tilde{R}\right)}{\tanh(b)}, \tag{3.6}$$

$$\tilde{v}_0 \tilde{R} \frac{\ln[\cosh(b)]}{b\tanh(b)} = \left[\tilde{f}_{\rm tot} - \tilde{\eta}_p \tilde{v}_0\right] + \nu - 1, \tag{3.7}$$

that can be solved numerically for $\tilde{v}_0$, the velocity at the pore entrance. Here, b is a (fixed) dimensionless parameter related to the spatial dependence of the velocity, and ensures global conservation of mass (see Publication III for details). In the SF regime, the line density at the pore

entrance is $\tilde{\sigma}_0 = 1$, since the stem close to the pore is in a single-file configuration. The effective friction is then given by

$$\tilde{\Gamma}(\tilde{t}) = \frac{\tilde{f}_{\rm tot}}{\tilde{\sigma}_0(\tilde{t})\tilde{v}_0(\tilde{t})}, \tag{3.8}$$

Finally, in the regime where the force is insufficient to straighten even a small part of the chain, $\tilde{f} \lesssim N^{-\nu}$, the chain adopts a trumpet-like shape. In this *trumpet* (TR) regime, the dynamics can be described by Eqs. (3.4)–(3.6), with the velocity $\tilde{v}_0$ and density $\tilde{\sigma}_0$ given by

$$\tilde{v}_0\tilde{R}\frac{\ln[\cosh(b)]}{b\tanh(b)} = \nu\left[\tilde{f}_{\rm tot} - \tilde{\eta}_p\tilde{v}_0\right]^{1/\nu}, \tag{3.9}$$

$$\tilde{\sigma}_0 = \left[\tilde{f}_{\rm tot} - \tilde{\eta}_p\tilde{v}_0\right]^{1-1/\nu}. \tag{3.10}$$

Note that Eqs. (3.7) and (3.9) ensure a smooth cross-over between the TR and SF regimes at $\left[\tilde{f}_{\rm tot} - \tilde{\eta}_p\tilde{v}_0\right] = 1$ and that the SF regime equations approach the SS regime Eq. (3.3) when $\tilde{f} \gg 1$ (as $\tilde{r} \to \tilde{R}$, $\tilde{\xi}_R \to 1$ and $b \to \infty$). In practice, the model consists of solving Eqs. (3.2) and (3.4)–(3.10), with Eqs. (3.9) and (3.10) chosen over Eq. (3.7) if $\left[\tilde{f}_{\rm tot} - \tilde{\eta}_p\tilde{v}_0\right] < 1$, and vice versa.

3.1.3 Physical basis of driven polymer translocation

In Publication III the BDTP model is compared against molecular dynamics (MD) simulations found in the literature. The main goal of the comparison is to show that the non-equilibrium tension propagation on the *cis* side subchain is the dictating physical process in driven polymer translocation, and that the BDTP model reproduces MD simulation results in a wide range of parameters and with quantitative accuracy. This goal has not been achieved by any previous theoretical model of driven translocation, despite the large variety of different approaches. However, in Publication III it is shown that by considering the tension propagation along the *cis* side subchain, it is possible to explain practically all available MD simulation results.

The most important and sensitive measure of translocation dynamics is the waiting time distribution. The waiting time distribution is defined as the time that each individual monomer spends inside the pore, and gives very detailed information about the translocation process. In Figure 3.3, the waiting time distribution as given by the BDTP model is compared with MD simulation results. As is shown, the match between BDTP and MD is almost exact. This agreement tells that the translocation dynamics

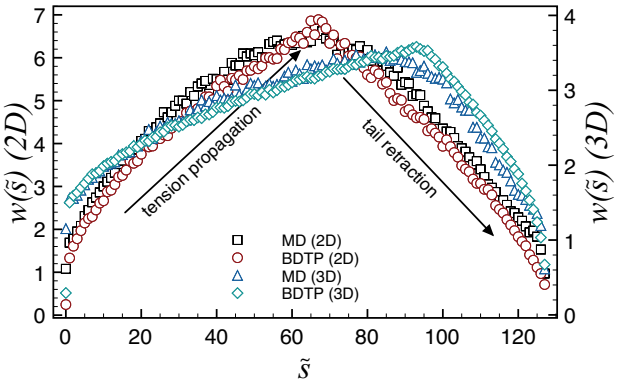

Figure 3.3. Comparison of waiting times w in both 2D and 3D for MD and the BDTP model. The agreement of the BDTP model with MD simulations is excellent, and reveals the two stages of translocation: the tension propagation stage of increasing $w(\tilde{s})$ and the tail retraction stage characterized by decreasing $w(\tilde{s})$. For direct comparison, the parameters used were the same for both MD and BDTP ($N = 128$, $f = 5$, $k_BT = 1.2$, $\eta = 0.7$), and the same number of statistical averages were used in both cases. The 3D MD results are from [66].

is reproduced correctly at the most fundamental level, which is of course a vital requirement for any theoretical model. The comparison also reveals a lucid picture of the translocation process: first, as tension propagates along the chain backbone, the effective friction increases and translocation slows down. In the second stage, the number of dragged monomers is reduced as the tail retracts, and translocation speeds up.

While the agreement shown in Figure 3.3 is remarkable, the comparison represents only one specific set of parameters. Any truly useful theory has to be able to cover a much larger regime of physical conditions. Since in most simulation studies the focus has been on obtaining the translocation time exponent α, the most comprehensive comparison between theory and existing simulations can be done by solving the translocation time as a function of chain length and by extracting the exponent α from those results. This comparison was done in Publication III, with the results reproduced in Table 3.1. The parameter range has been chosen to span the TR, SF and SS regimes, and to cover both short and long chain regimes in both 2D and 3D. Despite the diversity of α in the different regimes, the BDTP model gives an accurate estimate of α in all of them. This fact clearly shows, that while the values of α depend on several parameters, they all share a common physical basis: non-equilibrium tension propagation on the *cis* side subchain. The interesting question is then, what is the source of the diversity of α. Why a universal description of

Table 3.1. Values of α ($\tau \sim N^{\alpha}$) from the BDTP model as compared to the corresponding values from MD simulations.

α (BDTP)	α (MD)	Dimension and parameter values
		2D, $T = 1.2$, Ref. [61]
1.51 ± 0.02	1.50 ± 0.01	$f = 5.0$, $\gamma = 0.7$, $20 \leq N \leq 70$
1.71 ± 0.02	1.69 ± 0.04	$f = 5.0$, $\gamma = 0.7$, $500 \leq N \leq 800$
1.52 ± 0.02	1.50 ± 0.02	$f = 2.4$, $\gamma = 0.7$, $20 \leq N \leq 70$
1.71 ± 0.02	1.65 ± 0.04	$f = 2.4$, $\gamma = 0.7$, $500 \leq N \leq 800$
1.66 ± 0.02	1.64 ± 0.01	$f = 5.0$, $\gamma = 3.0$, $20 \leq N \leq 70$
1.71 ± 0.02	1.67 ± 0.03	$f = 5.0$, $\gamma = 3.0$, $500 \leq N \leq 800$
		3D, $T = 1.2$, Ref. [63]
1.59 ± 0.02	1.58 ± 0.03	$f = 0.5$, $\gamma = 0.7$, $16 \leq N \leq 128$
1.35 ± 0.02	1.37 ± 0.05	$f = 5.0$, $\gamma = 0.7$, $16 \leq N \leq 256$
1.34 ± 0.02	1.37 ± 0.02	$f = 10.0$, $\gamma = 0.7$, $16 \leq N \leq 256$
		3D, $T = 1.2$, Ref. [62]
1.41 ± 0.01	1.42 ± 0.01	$f = 5.0$, $\gamma = 0.7$, $40 \leq N \leq 800$
1.39 ± 0.02	1.41 ± 0.01	$f = 5.0$, $\gamma = 0.7$, $64 \leq N \leq 256$
		3D, $T = 1.0$, Ref. [47]
1.46 ± 0.02	1.47 ± 0.05	$f = 3.0$, $\gamma = 11.7$, $70 \leq N \leq 200$
1.49 ± 0.02	1.50 ± 0.01	$f = 30.0$, $\gamma = 11.7$, $200 \leq N \leq 800$

the physics gives clearly non-universal scaling exponents? The answer lies in the chain length regimes studied both in experiments and simulations. Typically, $N \lesssim 10^3$. However, this chain length is still far from the asymptotic limit. For driven polymer translocation, significant finite size effects persist for extremely long chains, even up to $N \approx 10^5$. Next, we will discuss the consequences of these finite size effects.

3.1.4 Non-universalities due to finite chain length effects

As was discussed in the previous Section, for relatively short chains the translocation dynamics is significantly affected by the pore friction η_p. On the other hand, for very long chains its contribution becomes negligible compared to the drag force of the *cis* side subchain. In that limit, according to Eqs. (3.7) and (3.9), the translocation velocity is $\tilde{v}_0(\tilde{t}) \propto \tilde{R}(\tilde{t})^{-1}$. The maximum waiting time, obtained when the tension front reaches the last monomer, i.e., $\tilde{R}(\tilde{t}_{\rm tp}) = \tilde{R}_{\rm eq} \sim N^{\nu}$, should therefore scale with chain length as $\tilde{w}_{\rm max} \propto \left[\tilde{v}_0(\tilde{t}_{\rm tp})\right]^{-1} \propto N^{\nu}$. In Publication IV this was found to be the case, as shown in Fig. 3.4. The figure displays the collapse of the waiting time distributions for different N onto a single master curve, implying that the scaling relation holds for large N. Since the area under the $w(\tilde{s})$ curve gives the average translocation time, one has $\tau \sim N^{\alpha}$ with $\alpha \approx 1 + \nu$. However, even for $N = 10^5$, the location of $w_{\rm max}$ slowly migrates to the right and the collapse to the master curve is not exact. This shows that even the chain length $N = 10^5$ is still not in the asymptotic limit! Consequently, for $N = 10^5$, the scaling of the average translocation time is also not exactly $\tau \sim N^{1+\nu}$. This is clearly seen in Figure 3.5, where the effective exponent $\alpha(N) \equiv \frac{d \ln \tau}{d \ln N}$ has been solved from the BDTP model up to $N \approx 10^{10}$. Asymptotically, the effective exponent approaches $\alpha(N \to \infty) = 1 + \nu$ in both 2D and 3D. However, the approach is exceedingly slow: in 3D, the effective exponent $\alpha(N)$ changes gradually even for $N = 10^{10}$.

Another illustration of the the non-universalities occurring due to finite chain length is the dependence of α on various parameters such as the driving force and pore diameter. Figure 3.6 shows $\alpha(N)$ solved for different driving forces $0.75 \leq \tilde{f} \leq 10$. Although the different forces trace out different curves for relatively small N, eventually they converge to $\alpha(N \to \infty) = 1 + \nu$. In the typical experimental or simulation regime, the exponent α retains its dependence on f, with α decreasing as f is increased. Similar dependence has been observed in MD simula-

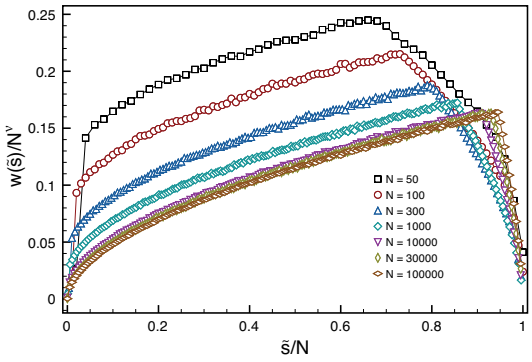

Figure 3.4. The waiting times per monomer $w(\tilde{s})$ in 3D as a function of monomer number $\tilde{s}$. In the long chain length limit, $w(\tilde{s}/N) \sim N^{\nu}$, implying the scaling $\tau \sim N^{1+\nu}$ for the mean translocation time. Model parameters used are $f = 5.0$, $k_B T = 1.2$, $\eta = 0.7$, $\nu = 0.588$ (3D).

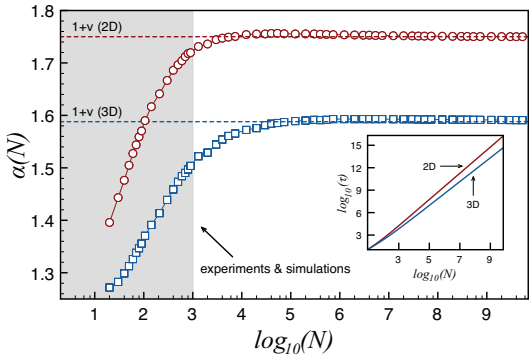

Figure 3.5. The effective exponent $\alpha(N) \equiv \frac{d \ln \tau}{d \ln N}$ in 2D (circles) and 3D (squares) as a function of N from the BDTP model, showing the extremely slow approach to the asymptotic limit $\alpha = 1 + \nu$. Most of experimental and simulation studies in the literature involve chain lengths of $N \lesssim 10^3$ (shaded region), being clearly in the finite chain length regime. The inset shows the raw data $\tau(N)$. Model parameters are the same as in Fig. 3.3.

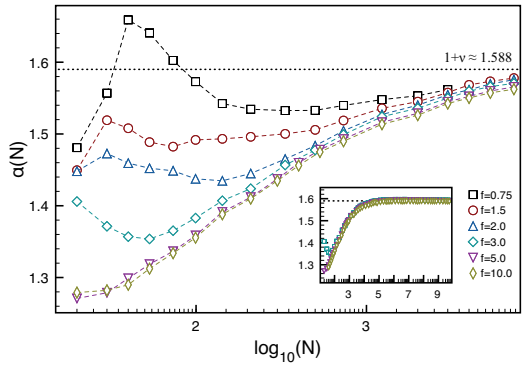

Figure 3.6. The effective exponent $\alpha(N)$ as a function of chain length N for the BDTP model solved for driving forces $f = 0.75, 1.5, 2.0, 3.0, 5.0, 10.0$. Other parameters are $k_BT = 1.2$, $\eta = 0.7$, $\eta_p = 5.0$. Errors are of the order of the symbol size. Inset: $\alpha(N)$ for $f = 3.0, 5.0, 10.0$ up to $N = 10^{10}$, showing the approach to the asymptotic value $\alpha(N \to \infty) = 1 + \nu$.

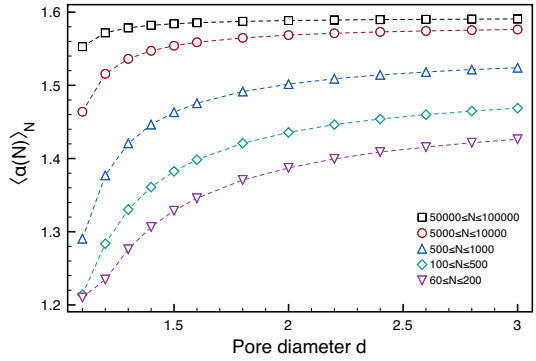

Figure 3.7. The effective exponent $\alpha(N)$ averaged over different chain length regimes shown as a function of pore diameter d. Model parameters are the same as in Fig. 3.4.

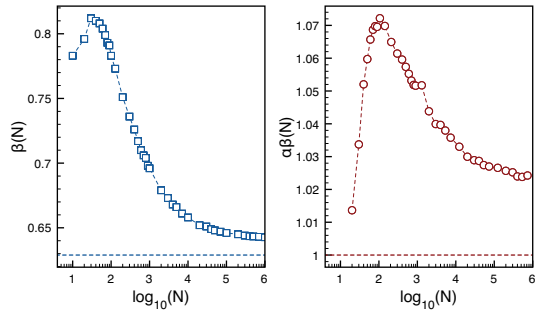

Figure 3.8. The exponent β ($\langle \tilde{s}(t) \rangle \sim t^{\beta}$, left panel) and the product of the exponents α and β (right panel) as a function of chain length. The dashed horizontal line shows the theoretical asymptotic ($N \to \infty$) limit. Model parameters are the same as in Figure. 3.4.

tions [63], although some authors report exactly opposite dependence of α on f [47, 60]. However, as argued in Publication IV, the latter simulations do not correspond to the canonical driven translocation problem, where the polymer initially starts from the *cis* side and has a finite probability to slip out of the pore back to *cis* side. Therefore, those results are not directly comparable with the BDTP model, or any other theories of driven translocation.

To show the effect of the pore size, the BDTP model was solved for different pore friction parameters, corresponding to various diameters of a circular pore of length a. As shown in Figure 3.7, for short chains the pore diameter has a large effect on the exponent α, while for long chains the effect becomes negligible, finally vanishing in the asymptotic limit. The correspondence between the pore diameter and pore friction is explained in more detail in Publication IV. Essentially, the translocation time can written as a sum of two terms, $\tau = AN^{1+\nu} + B\tilde{\eta}_p N$. The first term corresponds to the drag force due to the *cis* side subchain, while the latter is due to the pore polymer interactions, characterized by the pore friction $\tilde{\eta}_p$. For very small pore diameters, the pore friction is extremely large, and one approaches the translocation time scaling $\tau \sim N$ suggested by Muthukumar [43]. However, with a fixed pore diameter, this scaling cannot hold asymptotically due to the diminishing contribution of the second term, and the scaling exponent gradually approaches the asymptotic value $1 + \nu$, as was shown in Figure 3.5.

As one more example of the finite size effects, the scaling exponent β was studied in Publication IV. The exponent β relates the mean value of the translocation coordinate s to time as $\langle s(t) \rangle \sim t^{\beta}$. Since at the moment of

translocation $s(t = \tau) = N$, the exponents α and β are related as $\alpha\beta = 1$. However, since the scaling $\langle s(t)\rangle \sim t^{\beta}$ is never exact for finite chains, the relation $\alpha\beta = 1$ can hold only asymptotically. Both the exponent β and the product $\alpha\beta$ approach the asymptotic limit extremely slowly, as shown in Figure 3.8. In the regime, where MD simulation data is available, the match between BDTP and MD is excellent (see Publication IV).

3.1.5 Limitations of the present theory

Although translocation dynamics has been shown in Publications III & IV to be dominated by the pore friction and the tension propagation on the *cis* subchain, the tension propagation theory also has some limitations. Neglecting the *trans* side subchain, although a very good approximation in the typical experimental and simulation regimes, may be an inadequate approximation in some limits. For example, for very high forces and short to intermediate chains when the system is well in the strong stretching regime, the translocation velocity is larger than the diffusive motion on the *trans* side. This leads to a build-up of monomer density near the pore on the *trans* side. This monomer crowding may have a non-negligible effect on the translocation velocity, and in the high-force regime, there are some indications that this may be the case. In Publication IV, the scaling exponent δ, which relates the translocation time to the driving force by $\tau \sim f^{\delta}$, was determined for both the theory and from MD simulations. While the theory and simulations give excellent agreement in the low to intermediate force regime, for high forces the exponent measured from MD simulations was slightly larger (-0.9 vs. -1.0). This indicates that in this regime, translocation occurs slightly slower than predicted by the theory and may be caused by the a non-negligible friction from the *trans* side subchain.

Another limitation of the present theory is related to the fluctuations of the translocation coordinate s and the distribution of translocation times. As discussed in Publication IV, the fluctuations are larger and the distribution correspondingly wider when obtained from MD simulations. At least one obvious reason for the diminished fluctuations is the complete absence of the *trans* side chain. Including the additional noise from the translocated part of the chain could bring both the scaling of the fluctuations of s and the distribution of translocation times closer to the MD results. However, a proper implementation of the *trans* side fluctuations would also require considering the out-of equilibrium effects of monomer

crowding in front of the *trans* side pore entrance.

Finally, for semi-flexible polymers neglecting the *trans* side subchain may not be a good approximation if the bending stiffness is very large. In that case, the polymer behaves almost as a rigid rod, and the subchain on the trans side contributes significantly to the overall friction. The approach to this limit from the flexible chain regime is not clear. A rigorous description of the transition from the flexible chain regime to the rigid rod regime would also require describing the non-equilibrium crowding near the *trans* side pore entrance, since at intermediate bending rigidity the friction due to the locally increased density may be important. However, this study is not within the scope of this Thesis.

3.2 Polymer translocation under time-dependent force

Most of the experimental and theoretical studies of driven polymer translocation have considered the process occurring under static, time-independent forces. However, in the biological environment, the forces can be time dependent due to fluctuations in the membrane potential, fluid density, ion concentration, etc. Therefore, to understand processes *in vivo*, it is important to study the effect of time-dependent fluctuations of the driving force on the translocation dynamics. Previously, the problem has been studied theoretically by Park & Sung for a dichotomically flipping force, whose time-dependent part changes its sign at certain average flipping rate. It was found that the translocation time obtains a minimum at a certain optimal flipping rate [67]. Notably, the translocation time can be smaller than in the absence of the time-dependent force, even when the mean of the time-dependent part of the force is zero. This is the resonant activation phenomenon that was discussed in Section 1.2.

In Publication V, the resonant activation of polymer translocation is studied with numerical Langevin dynamics simulations. The equations of motion for the monomers are given by Eq. (2.1) in 2D, with the monomer-monomer interactions given by the FENE and the repulsive Lennard-Jones interactions discussed in Section 2.4. All monomer-wall particle pairs have the same short-range repulsive LJ interaction. In addition, two main types of interactions between the monomers and the pore particles are considered. In the first case, the pore particles are considered to be identical with the wall particles, having a purely repulsive interaction with the monomers. In the second case, the cut-off distance of the LJ

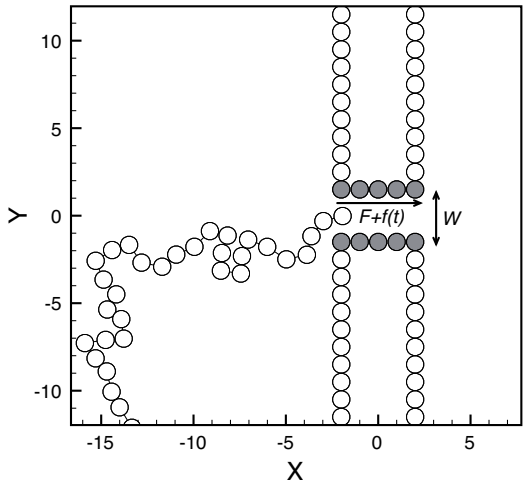

Figure 3.9. A schematic representation of the system used in the translocation simulations with time-dependent driving force. The polymer, placed initially on the *cis* side, is driven through the pore of length $L = 5$ and width $W = 3$ by the external force $F + f(t)$. The interaction between the pore monomers (shaded gray) and the polymer can be either repulsive or attractive (see text).

potential between monomer-pore particles is increased to 2.5σ (with $U_{\rm LJ}$ constant for $r > 2.5\sigma$), and the interaction strength is characterized by $\epsilon_{\rm pm}$. The interaction can be either attractive or repulsive, depending on the distance of the monomer from the pore particles. The pore with the larger cut-off is called attractive, while the one with the shorter cut-off is called repulsive.

In addition, when inside the pore, the monomers experience an external driving force $\mathbf{F}_{\rm ext} = [F + f(t)]\hat{x}$, where F is the static force, $f(t)$ is the time-dependent force and $\hat{x}$ is the unit vector along the direction of the pore axis. In Publication V, we have studied two types of time-dependent forces $f(t)$. The first is the dichotomic noise, for which $f(t)$ is either $+A_d$ or $-A_d$, and changes from one value to the other with flipping rate ω. The dichotomic $f(t)$ has zero mean and is exponentially correlated: $\langle f(t)\rangle = 0$ and $\langle f(t)f(0)\rangle = A_d^2 \exp(-2\omega t)$. As a second example, we have considered the sinusoidal force given by $f(t) = A\sin(\omega t + \phi)$, where A is the amplitude, ω the angular frequency and ϕ is a constant phase. While the first one may be more realistic description of non-equilibrium fluctuations in biological system, the periodic sinusoidal force is easier to implement experimentally. Other simulation details can be found in Publication V.

It is shown in Publication V that the polymer translocation exhibits the resonant activation phenomenon similar to the Kramers problem, but

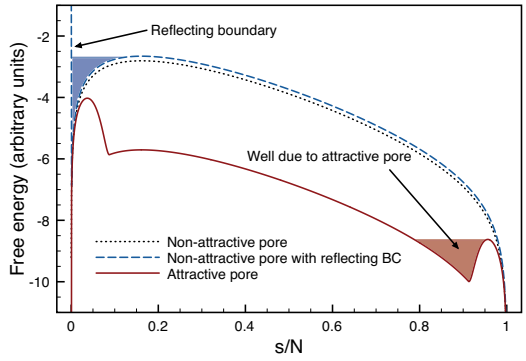

Figure 3.10. Illustration of the free energy of the polymer chain as a function of the number of translocated monomers s. The dotted line indicates the free energy for the non-attractive pore, which has no well structure (cf. Figure 1.6). A reflecting boundary condition at $s = 0$ forms a free-energy well (blue shaded area). Attractive polymer-pore interactions can also create a free-energy well (schematically shaded red).

only under certain conditions. As we mentioned in Section 1.2, the existence of the minimum residence time relies on the system's initial state having a significant proportion of states with the barrier in the upper position. It turns out that for the polymer translocation problem, this requirement is only satisfied if there is a sufficiently strong attraction between the pore and the polymer. This is because the free energy landscape of the translocation problem is markedly different from the metastable Kramers' potential. Without the attractive interactions, the free energy barrier of a translocating polymer has a maximum, but no finite minima (see Figure 3.10). Consequently, for low flipping rates and when the barrier is initially in the upper state, the system cannot simply wait in the metastable well until the crossing occurs due to thermal fluctuations or barrier flipping. Instead, the thermal fluctuations drive the polymer out of the pore to the *cis* side, towards the free energy infimum. These failed translocation events do not count towards the average of translocation time, which is typically (in both experiments and simulations) calculated over the ensemble of successful translocations. In this ensemble, the probability that the barrier is initially in the upper position becomes negligible for sufficiently high amplitudes of the dichotomic force. Therefore, the conditions for the resonant activation are not met and the phenomenon does not occur.

In the case of the theoretical study by Park & Sung [67], a reflecting boundary condition was used, which essentially prevents the chain escape to the *cis* side. As illustrated in Figure 3.10, this creates a free-energy

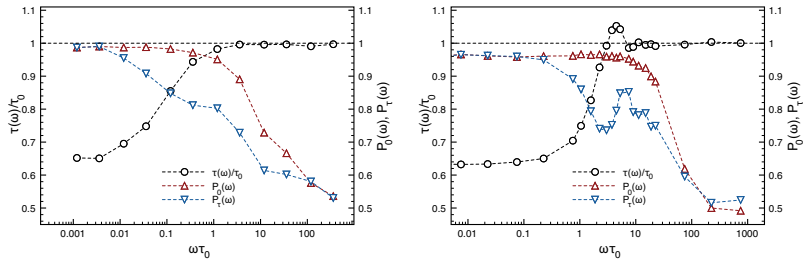

Figure 3.11. The mean translocation time τ and the probabilities P_0 and P_τ that the force $f(t)$ is positive for $t = 0$ and $t = \tau$ as a function of ω for the dichotomic $f(t)$ (left panel) and the sinusoidal $f(t)$ (right panel). $\tau_0 \approx 750$ is the translocation time with $f(t) \equiv 0$. Simulations parameters are $T = 1.2$, $\eta = 0.7$, $F = 0.3$, $A_d = 0.2$ (dichotomic force) and $A = 0.3$ (sinusoidal force).

landscape similar to the Kramers problem, for which resonant activation exists. Similarly, the attractive interaction between the pore and the polymer, if strong enough, prevents the escape to the *cis* side and the resonant minimum in translocation time appears. However, in this case the relevant barrier crossing process is not the translocation as a whole, but only the very last stages, when the polymer is already almost completely on the *trans* side. The attractive interaction makes also the escape to the *trans* side an activated barrier crossing process (see Figure 3.10). However, because of the forward bias due to the external driving force, the escape to the *trans* side is much probable than to the *cis* side.

Because of the qualitative differences of the translocation process with the non-attractive and attractive pore-polymer interactions, the two are discussed separately below.

3.2.1 Non-attractive pore

For the non-attractive pore, resonant activation does not exist. Instead, the mean translocation time has a cross-over from a fast translocation regime at low flipping rates (angular frequencies for the sinusoidal force) to a slower translocation regime at high flipping rates (see Figure 3.11). In the fast regime, mean translocation time τ is shorter than the translocation time in the absence of the time-dependent force, τ_0. The average is dominated by the events where the time-dependent force is in the forward direction, $f(t) > 0$, because the translocation probability increases strongly with the driving force. This is also shown in Figure 3.11, where the probabilities $P_0 \equiv P[f(0) > 0]$ and $P_\tau \equiv P[f(\tau) > 0]$ that the force $f(t)$ is positive for $t = 0$ and $t = \tau$, respectively, are plotted as a function of ω.

In the high-ω regime, the effect of the time-dependent force is averaged out, and $\tau \approx \tau_0$. Between the two limits, the system with dichotomic $f(t)$ has a smooth cross-over from one regime to the next. However, the system with the sinusoidal $f(t)$ shows much richer behavior. Instead of a simple cross-over in $\tau(\omega)$, one gets a series of local minima and maxima. In addition, the probability P_τ has a local maximum in the vicinity of a local minimum of τ. In many cases, these could be argued to indicate resonant activation [22]. However, it is shown in Publication V that in this case they have a purely deterministic origin. The results are in fact nicely reproduced by a simple deterministic model for the translocation coordinate s,

$$\eta_{\text{eff}} \frac{d\langle s(t)\rangle}{dt} = F\left[1 + \sin(\omega t + \phi)\right]. \tag{3.11}$$

In Eq. (3.11) η_{eff} is the effective friction that sets the time scale of the system[1]. Eq. (3.11) can be analytically solved to give the translocation time as function of the phase,

$$\tau(\phi) = \tau_0 + \frac{1}{\omega}\left[\cos(\omega\tau + \phi) - \cos(\phi)\right]. \tag{3.12}$$

The average translocation time is then found by taking the average of $\tau(\phi)$ over the distribution of ϕ as

$$\tau = \frac{1}{2\pi}\int_0^{2\pi} p(\phi)\tau(\phi)d\phi. \tag{3.13}$$

The behavior of τ as a function of ω closely depends on the form of the distribution $p(\phi)$. For the uniform distribution, $\tau(\omega)$ displays a minimum characteristic of resonant activation. Similar results have been reported in several polymer systems that have been used as analogues of polymer translocation [68, 69, 70]. However, this type of behavior is in sharp contrast with the simulation results of Publication V. This demonstrates the shortcomings of the model systems with respect to polymer translocation and underlines the importance of the realistic free-energy barrier. For the non-attractive pore, the free-energy has no metastable state, and therefore the chain can escape to the *cis* side. Because of this, the initial states corresponding to negative $f(t)$ are mainly absent from the distribution

[1] As discussed earlier in the context of the tension propagation theory, the effective friction in driven translocation is not constant in time. However, for the purposes of the model of Eq. (3.11), assuming constant η_{eff}, although a crude approximation, is sufficient. In addition, in the present case the time-dependent driving force induces strong back-and-forth motions of the chain. Without also considering the *trans* side non-equilibrium configurations, it is not possible to take this into account within the tension propagation theory.

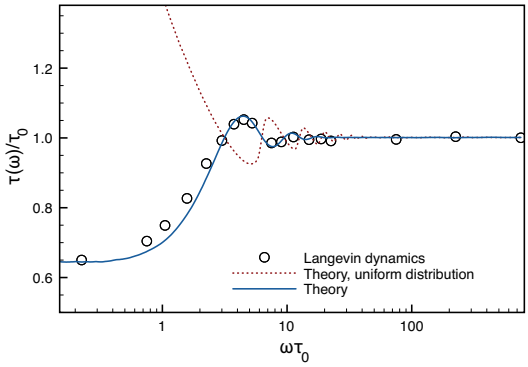

Figure 3.12. Comparison between LD simulations and the theoretical model of Eqs. (3.11) and (3.13). Dotted line: with uniformly distributed ϕ, solid line: with non-uniformly distributed ϕ (see text and Publication V). The latter shows good agreement with the Langevin dynamics results (circles).

$p(\phi)$. Taking this into account in Eq. (3.13) gives a very nice agreement with the simulations, as shown in Figure 3.12. This shows that in the case of the repulsive pore, there is no resonant activation for polymer translocation, and that the main features can be explained by simple deterministic arguments.

3.2.2 Attractive pore

If the interactions between the pore and the polymer are attractive, the translocation dynamics change in several ways. First, the mean translocation time $\tau(\omega)$ now has a global minimum, characteristic of resonant activation (see Figure 3.13). The resonance is due to the qualitative change in the free energy, shown in Figure 3.10, that is promoted by the attractive interactions. For sufficiently strong attraction, the escape of the chain to the *cis* side becomes extremely rare and, correspondingly, the translocation to the *trans* side becomes an activated process. Because of the lack of escapes to the *cis* side, for small ω the mean translocation time is dominated by the events occurring with negative $f(t)$ (but positive $F + f(t)$). Since, for the attractive pore, the final escape to the *trans* side is a thermally activated event, the corresponding escape time depends exponentially on the value of $f(t)$, similarly to the Kramers' problem. Therefore, the translocation time in the $\omega \to 0$ limit is larger than τ_0. This is in sharp contrast to the results of the repulsive pore, where $\tau(\omega \to 0) < \tau_0$. For the high-$\omega$ regime, on the other hand, the behavior is similar to the non-attractive case. Here, the fast fluctuations in $f(t)$ are averaged out,

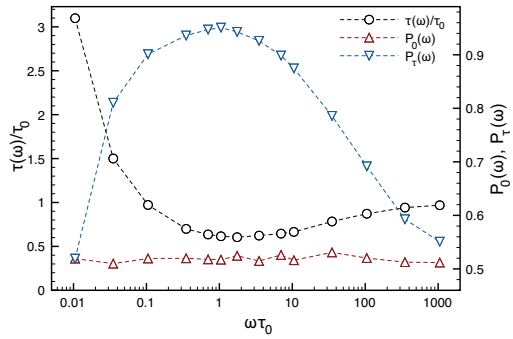

Figure 3.13. The mean translocation time τ and the probabilities P_0 and P_τ for the dichotomic force and attractive pore. The simulation parameters are $N = 32$, $F = 0.5$, $A_d = 0.2$, $\epsilon_{\rm pm} = 2.5$, and $\tau_0 \approx 2202 \pm 29$.

and one has $\tau \approx \tau_0$. Between the high and low flipping rate limits is the region of fast translocation with $\tau < \tau_0$, with the resonant minimum located approximately at $\omega\tau_0 \approx 1$.

The probabilities P_0 and P_τ also show the qualitative change in the dynamics. For the non-attractive pore and dichotomic driving force, both probabilities monotonically decrease from $P_0(\omega \to 0) = P_\tau(\omega \to 0) \approx 1$ to $P_0(\omega \to \infty) = P_\tau(\omega \to \infty) \approx 0.5$ as ω is increased. This is because of the increasing number of failed translocations (escapes to the *cis* side) for low ω. However, for sufficiently strong attractive interactions, most of the translocation events result in a success. Therefore, the probability $P_0(\omega)$ to have initially $f(0) > 0$ is roughly 0.5 and independent of ω, i.e., there is almost no selection with respect to the initial state of the time-dependent force. The probability P_τ, on the other hand, depends strongly on ω, having a maximum near the resonant flipping rate. This is a characteristic sign of resonant activation. At this value of ω, the flipping rate synchronizes with the barrier crossing rate, and most of the successful translocations occur when $f(\tau) > 0$, i.e., when the barrier is in the lower position. This kind of behavior defines the resonant activation phenomenon, as we discussed in the context of the Kramers' problem in Section 1.2.

What distinguishes the resonant activation in polymer translocation from other typical resonant activation phenomena, is that in polymer translocation, only part of the process responds to the time-dependent force to produce the resonance. To see this, we divide the translocation process into three subprocesses: 1) the initial filling of the pore, 2) transfer of the polymer from the *cis* side to the *trans* side and 3) the final emp-

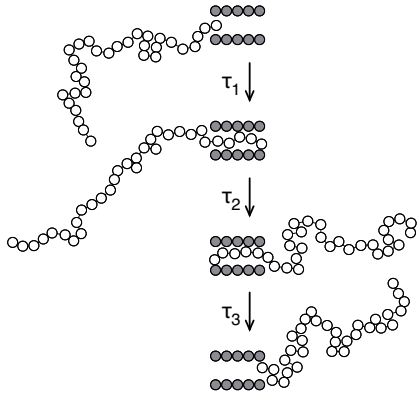

Figure 3.14. The translocation process divided into three stages: 1) initial filling of the pore, 2) transfer of the polymer from the *cis* side to the *trans* side, 3) the final emptying of the pore. The corresponding times of the subprocesses are τ_1, τ_2 and τ_3, with the total translocation time $\tau = \tau_1 + \tau_2 + \tau_3$.

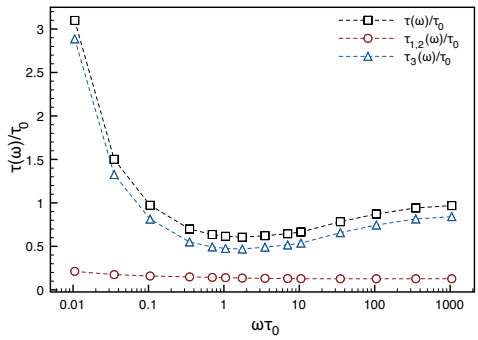

Figure 3.15. The mean translocation time τ, the pore emptying time τ_3 and the time $\tau_{1,2} = \tau_1 + \tau_2$ ($= \tau - \tau_3$) for the dichotomic force and attractive pore. Parameters are the same as in Figure 3.13.

tying of the pore. (see Figure 3.14)[2]. The times corresponding to these subprocesses are τ_1, τ_2 and τ_3, respectively. The total translocation time is then given by $\tau = \tau_1 + \tau_2 + \tau_3$. For the attractive pore with $\epsilon_{\rm pm} = 2.5$, the translocation time τ and the times $\tau_{1,2} \equiv \tau_1 + \tau_2$ and τ_3 are shown in Figure 3.15. Remarkably, the time $\tau_{1,2}$ is almost independent of the flipping rate, only slightly decreasing with ω. The pore-emptying time τ_3, on the other hand, depends strongly on ω, having a minimum close to $\omega\tau_0 = 1$. This shows that for the resonant activation, the relevant process is not the whole translocation, but only the last pore emptying process. This is of course natural, since the activation barrier introduced by the attractive polymer-pore interactions corresponds to this last stage of translocation (see Figure 3.10).

Since the relevant process for the resonant activation is the pore emptying process, the resonant flipping rate depends only weakly on the chain length. This is because the chain length influences the barrier height only through the chain's entropy, which is typically small compared to the attractive interaction. However, because the time $\tau_{1,2}$ increases with chain length roughly as $\tau_{1,2} \sim N^{1.5}$ [74], the relative contribution of τ_3 to the total translocation time τ gets smaller for long chains. Therefore, the resonance is strongest for short chains, as is shown in Figure 3.16, where $\tau(\omega)$ is computed for $16 \leq N \leq 128$. On the other hand, increasing the static driving force F has a big effect on both the resonant flipping rate and the depth of the resonant minimum. For large forces, the barrier becomes very small, which leads to larger crossing rate and the resonance appearing at a higher flipping rate. In addition, the minimum becomes shallower, because the relative importance of τ_3 is smaller. Finally, when the barrier becomes small enough, the resonance practically vanishes (see Figure 3.17). Similarly, for very large amplitudes of the dichotomic force, the resonance vanishes (see Figure 3.18). In this case the reason is, however, different. As the amplitude gets larger than the static force, $A_d > F$, the number of failed translocations, especially for small ω, starts to increase. For sufficiently large A_d, most translocation attempts in the low-ω regime starting with $f(0) = -A_d$ fail, and the system effectively goes back to the non-attractive limit.

Under the sinusoidal driving force, the general behavior of the system is similar to the dichotomic force. The main features are governed by the

[2]Same kind of division has been used in Refs. [71, 72, 73, 74, 75] to analyze translocation through an attractive pore with a static driving force.

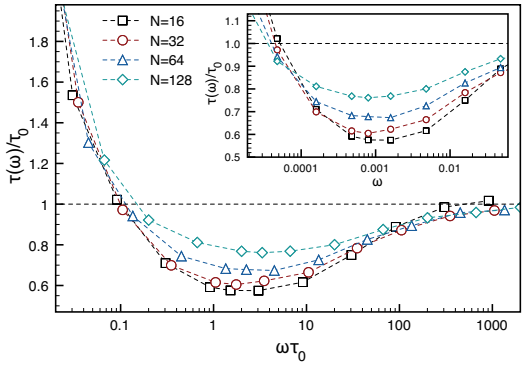

Figure 3.16. Translocation times for chain lengths $16 \leq N \leq 128$ with the dichotomic force and attractive pore. $F = 0.5$, $A_d = 0.2$ and $\epsilon_{\rm pm} = 2.5$. While the optimal rescaled flipping rate ($\omega\tau_0$) shows a slight dependence on N (main figure), the unnormalized flipping rate (ω) is independent of N (inset).

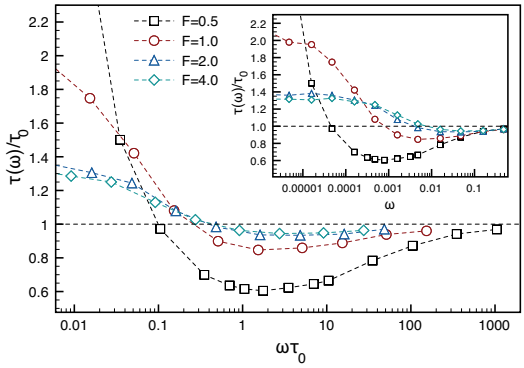

Figure 3.17. Translocation times for driving forces $0.5 \leq F \leq 4$ for the dichotomic force and attractive pore. $A_d = 0.4F$, $\epsilon_{\rm pm} = 2.5$. In this case, the optimal rescaled flipping rate ($\omega\tau_0$) is roughly independent of F (main figure), while the unnormalized flipping rate (ω) strongly increases with F (inset)

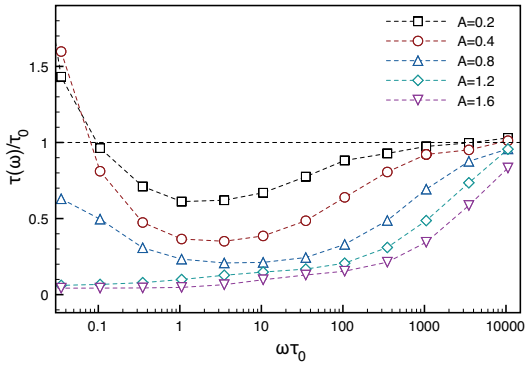

Figure 3.18. Translocation times for the dichotomic force and attractive pore for amplitudes $A_d \in \{0.2, 0.4, 0.8, 1.6\}$. $F = 0.5$, $\epsilon_{\rm pm} = 2.5$.

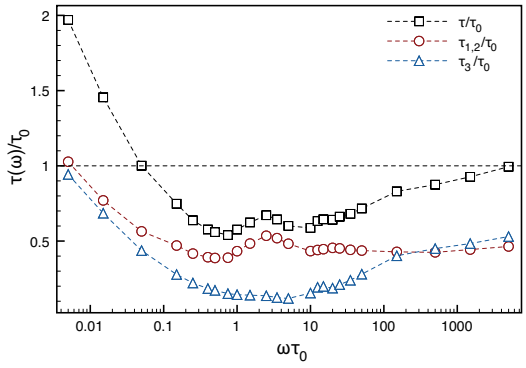

Figure 3.19. The translocation time τ and its components $\tau_{1,2}$ and τ_3 as a function of ω, showing that the leftmost minimum in $\tau(\omega)$ is associated with $\tau_{1,2}$. Parameter values used are $F = 0.5$, $A = 1.0$, $\epsilon_{\rm pm} = 2.0$ and $N = 32$.

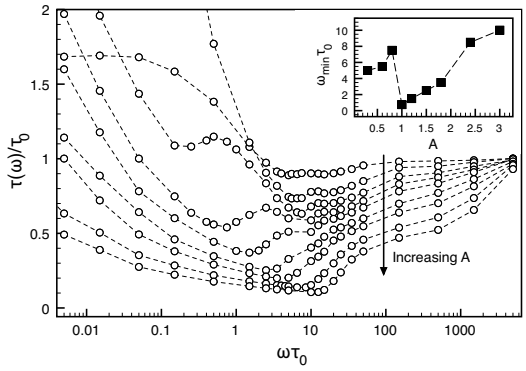

Figure 3.20. Translocation time τ as a function of frequency ω for the periodic driving force $f(t) = A\sin(\omega t + \phi)$ for amplitudes $A \in \{0.3, 0.6, 0.8, 1.0, 1.2, 1.5, 1.8, 2.4, 3.0\}$. Other parameters are $F = 0.5$, $\epsilon_{\rm pm} = 2.0$ and $N = 32$. The inset shows the dependence of the frequency $\omega_{\rm min}$ of the global minimum translocation time on the amplitude A. Here $\tau_0 \approx 500 \pm 6$.

pore emptying process, leading to very similar behavior of $\tau(\omega)$ as a function of chain length, driving force and attraction strength. However, the periodic force also weakly couples to the overall motion of the chain, producing a set of local minima and maxima, similar to the non-attractive pore. Since the source of these extrema is the overall back-and-forth motion of the chain, they are visible in the time $\tau_{1,2}$ rather than in τ_3, as shown in Figure 3.19. Because of this additional coupling of $f(t)$ to the time $\tau_{1,2}$, a rather complicated behavior arises as the amplitude A of the sinusoidal force is increased. Figure 3.20 summarizes the behavior for different A. As the amplitude A is increased, the resonant minimum becomes deeper and slowly moves toward higher frequencies, similar to the dichotomic $f(t)$. However, in addition to the original one, another (local) minimum appears at the low-frequency end of the spectrum and travels down the $\tau(\omega)$ curve as A is increased. Eventually, the new minimum becomes a global one. This produces a sudden transition in the frequency of minimum translocation time, $\omega_{\min}$, as shown in the inset of Fig. 3.20. Finally, at sufficiently large A, the new minimum merges with the original one. This behavior is analyzed in detail in Publication V, but essentially it arises because of two factors: the periodicity of the driving force, and the dependence of the distribution $p(\phi)$ on the frequency ω and the amplitude A. Thus, the cause is very similar to the oscillations of $\tau(\omega)$ for the non-attractive pore, although because of the attractive interaction and the resulting free-energy barrier the system cannot be analyzed by deterministic models such as Eq. (3.11).

4. Summary and outlook

The main results of this Thesis are related to the theoretical understanding of polymer translocation, a process which is of both theoretical and practical interest due to its applications in DNA sequencing and biotechnology. In this Thesis, we show that the driven polymer translocation problem can be accurately described by the so-called tension propagation theory, and that finite size effects due to pore-polymer interactions prevail well beyond the experimentally and numerically relevant chain length regimes. We have also considered the translocation of a polymer under a time-dependent force by Langevin dynamics simulations, and show that also in this case the pore-polymer interactions can even change the qualitative nature of the process. In addition to the polymer translocation, we have studied a related problem, namely the escape of a polymer chain from a metastable state. In this context, we have employed and further developed the Path Integral Hyperdynamics method, which we showed to give significant speed-up in computations of rare event problems.

The importance of the polymer escape study presented in Publications I & II is twofold. First, in Publication I, the PIHD method is studied and it's computational speed-up is measured and quantitatively analyzed. While the speed-up can be several orders of magnitude, the inefficiency of transition path sampling at large bias forces reduces the speed-up significantly. In addition, the dramatic difference in the efficiency of the different biasing schemes – and especially in the noisiness of the normalization factor – suggests the existence of an optimal bias potential. While the non-monotonic dependence of the boost factor on the bias amplitude was demonstrated in Publication I, the existence of a bias function that gives the globally optimal computational boost remains an open question. Because of both theoretical and practical implications, it would be an interesting topic for future research. The polymer escape problem studied

in Publication II showed not only the PIHD method's applicability to more complex systems, but also provided interesting details about the modeling and physics of polymer chains. According to the study, the widely used ideal chain approximation, although more amenable to analytical calculations, may be an inadequate description of the polymer's properties when the size of the polymer is comparable to the system's characteristic length scale. Here, the excluded volume interactions and finite flexibility can have a large effect on the polymer's dynamics. The study also suggests that sorting polymers according to length and bending rigidity should be possible with an external force field, due to the non-monotonic dependence of the escape rate on the chain length and bending rigidity.

In Publications III & IV, the theory of driven polymer translocation is studied. Until very recently, several competing theories of the process existed, none of them able to claim very good agreement with simulations or experiments. The major achievement of Publication III is to show that the accurate physical description of driven polymer translocation is given by the tension propagation theory. The theory is further investigated in Publication IV, where the nature of finite size effects is studied. This work reveals the importance of polymer-pore interactions and the post-propagation stage for finite chain lengths, and shows that the finite size effects can persist for extremely long chains, well beyond the regime available to experiments and simulations. Despite the significant advances, several interesting details remain to be studied. For example, the inclusion of hydrodynamic (Zimm) friction to the theoretical model is possible, and it would be interesting to see what the effect of hydrodynamic interactions is, when the finite chain length effects are properly taken into account. This work is planned for the near future, and should help bridge the gap between the simulations and experiments.

The influence of the pore-polymer interactions on the translocation dynamics is further studied in Publication V. This time, a time-dependent driving force is considered, motivated by the non-equilibrium fluctuations encountered in biological systems, and by the possibility to use a time-dependent driving force in experimental setups for polymer separation or identification. It is shown that the non-equilibrium fluctuations can significantly speed up polymer translocation, and, provided that there is a strong enough attraction between the pore and the polymer, may induce a resonant activation in the system, where the translocation time attains a minimum at finite frequency of the non-equilibrium noise. In this spe-

cial case of polymer translocation, one has a thermally activated process similar to the polymer escape problem.

Finally, there is a class of polymer translocation problems that is outside the scope of this Thesis, namely the unbiased polymer translocation. In this case, there is no net external driving force on the polymer, and translocation is governed by thermal fluctuations arising from the surrounding solvent. Although the problem has been studied extensively in the literature, both with theory and simulations (cf. Ref. [76] for a review), the results presented in this Thesis cast these previous studies in a new light. For the driven translocation, the finite chain length effects due to the pore may persist even for chain lengths up to $N = 10^5$. It is therefore conceivable that the previous studies of unbiased translocation may be subject to similar finite size effects. Therefore, also the unbiased translocation problem deserves to be revisited from a new perspective, where the finite size effects are taken into account. A first step towards such an attempt was made by de Haan and Slater [77] in a simulation study, but the question of finite size effects in this case remains largely unanswered. The main obstacle in a simulation study is the enormous computational effort required to study long chains. It is possible that the PIHD method could be used to speed up the unbiased translocation by introducing a small hyperdynamics bias. This endeavor, however, is a subject of future research.

Bibliography

[1] F. Sanger, G.M. Air, B.G. Barrell *et al.*, Nature **265**, 687 (1977).

[2] R.D. Fleischmann, M.D. Adams, O. White *et al.*, Science **269**, 496 (1995).

[3] E.S. Lander, L.M. Linton, B. Birren *et al.*, Nature **409**, 860 (2001).

[4] J.C. Venter, M.D. Adamas, E.W. Myers *et al.*, Science **291**, 1304 (2001).

[5] E.E. Schadt, S. Turner and A. Kasarskis, Hum Mol Gen **19**, R227 (2010).

[6] E.R. Mardis, Nature **470**, 198 (2011).

[7] M. Akeson, D. Branton, J.J. Kasianowicz *et al.*, Biophys J **77**, 3227 (1999).

[8] A. Meller, L. Nivon, E. Brandin *et al.*, Porc Natl Acad Sci USA **97**, 1079 (2000).

[9] D. Branton, D.W. Deamer, A. Marziali *et al.*, Nature Biotech. **26**, 1146 (2008).

[10] Press release by Oxford Nanopore Technologies, 17th February 2012, available at: *http://www.nanoporetech.com/news/press-releases/view/39*. Accessed 9th March 2012.

[11] P. Hänggi, J Stat Phys **42**, 105 (1986).

[12] W.T. Coffey, Y.P. Kalmykov and J.T. Waldron, *The Langevin Equation With Application to Stochastic Problems in Physics, Chemistry and Electrical Engineering*, 2nd edition (World Scientific, 2005).

[13] H. Risken, *The Fokker-Planck Equation: Methods of Solution and Applications*, 2nd edition (Springer-Verlag, 1996).

[14] H. A. Kramers, Physica (Utrecht) **7**, 284 (1940).

[15] D. Chandler, *Introduction to Modern Statistical Mechanics* (Oxford University Press, 1987).

[16] C. Dellago, P.G. Bolhuis, F.S. Csajka, D. Chandler, J. Chem. Phys. **108**, 1964 (1998).

[17] P. Hänggi, P. Talkner and M. Borkovec, Rev Mod Phys **62**, 251 (1990).

[18] A.F. Voter, J. Chem. Phys. **106**, 4665 (1997).

[19] K. Binder and D.W. Heermann, *Monte Carlo Simulation in Statistical Physics, An Introduction*, 5th edition (Springer, 2010).

[20] A.F. Voter, F. Montalenti and T.C. Germann, Annu. Rev. Mater. Res. **32**, 321 (2002).

[21] L.Y. Chen and N.J.M. Horing, J. Chem. Phys. **126**, 224103 (2007).

[22] C. R. Doering and J. C. Gadoua, Phys. Rev. Lett. **69**, 2318 (1992).

[23] M. Boguna, J.M. Porra, J. Masoliver and K. Lindenberg, Phys. Rev. E **57**, 3990 (1998).

[24] C. Schimitt, B. Dybiec, P. Hänggi and C. Bechinger, Europhys. Lett. **74**, 937 (2006).

[25] P. J. Park and W. Sung, J. Chem. Phys. **111**, 5259 (1999).

[26] S. Lee and W. Sung, Phys. Rev. E **63**, 021115 (2001).

[27] K. Lee and W. Sung, Phys. Rev. E **64**, 041801 (2001).

[28] K. L. Sebastian, Phys. Rev. E. **61**, 3245 (2000); K. L. Sebastian and Alok K. R. Paul, *ibid.* **62**, 927 (2000).

[29] K.L. Sebastian and A. Debnath, J. Phys. Condens. Matter **18**, S283 (2006).

[30] M. Doi, *Introduction to Polymer Physics* (Clarendon Press, 1996).

[31] J.J. Kasianowicz, E. Brandin, D. Branton and D.W. Deamer, Proc. Natl. Acad. Sci. USA **93**, 13770 (1996).

[32] M. P. Allen and D. J. Tildesley, *Computer Simulation of Liquids* (Oxford University Press, 1987).

[33] D.L. Ermak and H. Buckholtz, J. Comput. Phys. **35**, 169 (1980).

[34] A. Brünger, L. Brooks III and M. Karplus, Chem. Phys. Lett. **105**, 495 (1984).

[35] W.C. Swope, H.C. Andersen, P.H. Berens and K.R. Wilson, J. Chem. Phys. **76**, 637 (1982).

[36] J. Nummela and I. Andricioaei, Biophys. J **93**, 3373 (2007).

[37] M. Chaichian and A. Demichev, *Path Integrals in Physics, Volume I: Stochastic Processes and Quantum Mechanics* (Institute of Physics Publishing, 2001).

[38] H. Kleinert, *Path Integrals in Quantum Mechanics, Statistics, Polymer Physics, and Financial Markets* (World Scientific Publishing, 2003).

[39] R. Elber and D. Shalloway, J. Chem. Phys. **112** 5539 (2000).

[40] T. Ala-Nissilä, R. Ferrando and S.C. Ying, Adv. Phys. **51**, 949 (2002).

[41] H. Mökkönen, *Application of Path Integral Hyperdynamics to the Polymer Escape Problem*, special assignment, Aalto University School of Science (2012).

[42] W. Sung and P.J. Park, Phys. Rev. Lett. **77**, 783 (1996).

[43] M. Muthukumar, J. Chem. Phys. **111**, 10371 (1999).

[44] D.K. Lubensky and D.R. Nelson, Biophys. J. **77**, 1824 (1999).

[45] J. Chuang, Y. Kantor and M. Kardar, Phys. Rev. E **65**, 011802 (2001).

[46] Y. Kantor and M. Kardar, Phys. Rev. E **69**, 021806 (2004).

[47] V.V. Lehtola, R.P. Linna and K. Kaski, Phys. Rev. E **78**, 061803 (2008).

[48] V. Lehtola, R.P. Linna and K. Kaski, Europhys. Lett. **85**, 58006 (2009).

[49] V.V. Lehtola, K. Kaski, R.P. Linna, Phys. Rev. E **82**, 031908 (2010).

[50] A. Bhattacharya, W.H. Morrison, K. Luo, T. Ala-Nissila, S.-C. Ying, A. Milchev and K. Binder, Eur. Phys. J. E **29**, 423-429 (2009).

[51] A. Bhattacharya and K. Binder, Phys. Rev. E **81**, 041804 (2010).

[52] H. Vocks, D. Panja, G.T. Barkema and R.C. Ball, J. Phys. Condens. Matter **20**, 095224 (2008).

[53] J.L.A. Dubbeldam, A. Milchev, V.G. Rostiashvili and T.A. Vilgis, Europhysics Lett. **79**, 18002 (2007).

[54] R. Metzler and J. Klafter, Biophys. J. **85**, 2776 (2003).

[55] T. Sakaue, Phys. Rev. E **76**, 021803 (2007).

[56] T. Sakaue, Phys. Rev. E **81**, 041808 (2010).

[57] T. Saito and T. Sakaue, arXiv:1103.0620 (2011).

[58] T. Sakaue, in proceedings *The 5th Workshop on Complex Systems*, AIP CP, 982, 508 (2008).

[59] P. Rowghanian and A. Y. Grosberg, J. Phys. Chem. B (2011).

[60] J. L. A. Dubbeldam, V. G. Rostiashvili, A. Milchev and T. A. Vilgis, arXiv:1110.5763 (2011).

[61] I. Huopaniemi, K. Luo, T. Ala-Nissila and S.C. Ying, J. Chem. Phys. **125**, 124901 (2006).

[62] K. Luo, S.T.T. Ollila, I. Huopaniemi, T. Ala-Nissila, P. Pomorski, M. Karttunen, S.-C. Ying and A. Bhattacharya, Phys. Rev. E **78** 050901(R) (2008).

[63] K. Luo, T. Ala-Nissila, S.-C. Ying and R. Metzler, Europhys. Lett. **88**, 68006 (2009).

[64] R. Metzler and K. Luo, Eur. Phys. J. Special Topics **189**, 119 (2010).

[65] A. Bhattacharya, Physics Procedia **3**, 1411 (2010).

[66] K. Luo, private communication.

[67] P.J. Park and W. Sung, Int. J. Bifurcat. Chaos. **8**, 927 (1998).

[68] N. Pizzolato, A. Fiasconaro, D. Persano Adorno, and B. Spagnolo, Phys. Biol. **7**, 034001 (2010).

[69] A. Fiasconaro, J. J. Mazo, and F. Falo, Phys. Rev. E **82**, 031803 (2010).

[70] A. Fiasconaro, J. J. Mazo, and F. Falo, J. Stat. Mech.: Theory Exp. (2011) P11002.

[71] K. Luo, T. Ala-Nissila, S. C. Ying, and A. Bhattacharya, Phys. Rev. Lett. **99**, 148102 (2007).

[72] K. Luo, T. Ala-Nissila, S. C. Ying, and A. Bhattacharya, J. Chem. Phys. **126**, 145101 (2007).

[73] K. Luo, T. Ala-Nissila, S. C. Ying, and A. Bhattacharya, Phys. Rev. Lett. **100**, 058101 (2008).

[74] K. Luo, T. Ala-Nissila, S. C. Ying, and A. Bhattacharya, Phys. Rev. E **78**, 061918 (2008).

[75] K. Luo, T. Ala-Nissila, S. C. Ying, and A. Bhattacharya, Phys. Rev. E **78**, 061911 (2008).

[76] A. Milchev, J. Phys. Condens. Matter **23**, 103101 (2011).

[77] H.W. de Haan, G. Slater, Phys. Rev. E **81**, 051802 (2010).

Aalto-DD 72/2012

ISBN 978-952-60-4646-4
ISBN 978-952-60-4647-1 (pdf)
ISSN-L 1799-4934
ISSN 1799-4934
ISSN 1799-4942 (pdf)

Aalto University
School of Science
Department of Applied Physics
www.aalto.fi

BUSINESS +
ECONOMY

ART +
DESIGN +
ARCHITECTURE

SCIENCE +
TECHNOLOGY

CROSSOVER

DOCTORAL
DISSERTATIONS